Observations of asymmetry in contrasting wave-and tidally-dominated environments within a meso-tidal basin: implications for estuarine morphological evolution

----

Hunt, Stephen, Bryan, Karin R., Mullarney, JuliaC., and Pritchard, Mark.

----

authors affiliation

Corresponding Author

Stephen Hunt

E-mail:sh231@students.waikato.ac.nz

University of Waikato
Earth and Ocean Sciences
Private Bag 3105
Hamilton
Waikato
New Zealand
3240

Author

K. R. Bryan

E-mail:kbryan@waikato.ac.nz

University of Waikato
Private Bag 3105
Hamilton
3240
New Zealand

This article has been accepted for publication and undergone full peer review but has not been through the copyediting, typesetting, pagination and proofreading process which may lead to differences between this version and the Version of Record. Please cite this article as doi: 10.1002/esp.3985

Julia C. Mullarney

E-mail:juliam@waikato.ac.nz

University of Waikato
Coastal marine group
Private bag 3105
Hamilton
New Zealand
3216

Mark Pritchard

E-mail:mark.pritchard@niwa.co.nz

NIWA
Coasts and Oceans
Gate 10 Silverdale Road
Hillcrest
Hamilton
Waikato
New Zealand
3216

Abstract

Tides are often considered to be the dominant hydrodynamic process within mesotidal estuaries although waves can also have a large influence on intertidal erosion rates. Here, we use a combination of hydrodynamic measurements and sediment deposition records to determine the conditions under which observed waves are “morphologically significant”, in which case they influence tidal and suspended sediment flux asymmetry and subsequently infilling over geomorphological timescales. Morphological significant conditions were evaluated using data from contrasting arms in a dendritic mesotidal estuary, in which the orientation of the arms relative to the prevailing wind results in a marked difference in wave conditions, deposition rates and morphology. By defining the morphological significance of waves as a product of the magnitude of bed shear stress and frequency of occurrence, even small (but frequently occurring) winds are shown to be capable of generating waves that are morphologically significant given sufficient fetch. In the arm in which fetch length is restricted, only stronger but rare storm events can influence sediment flux and therefore tides are more morphologically significant over longer timescales. Water depth within this mesotidal estuary is shown to be a critical parameter in controlling morphological significance; the rapid attenuation of short period waves with depth results in contrasting patterns of erosion occurring during neaps and accretion during springs.

1 Introduction.

Tides and tidal asymmetry are essential drivers of sediment transport, morphological change and stability in estuarine environments (Friedrichs and Aubrey, 1988, Friedrichs, 2011). A system of non-linear feedbacks links tides and morphology, in which the tidal asymmetry affects sediment deposition patterns, and then the modified morphology further alters the asymmetry by distorting the tidal wave (e.g. Lanzoni and Seminara, 2002, Friedrichs, 2010).

Tidal asymmetry can affect sediment transport in two ways: (i) through an imbalance in maximum flow causing either the flood (flood dominant) or ebb (ebb dominant) currents to be stronger and (ii) through changes in the duration of time around slack water during which sediment can settle out of suspension and deposit on the seabed (Friedrichs, 2011). Intertidal areas in which the average water depth is deep relative to mean sea level (MSL) (such as in the case of a concave-shaped depth profile) will tend to slow the progression of low water (LW) relative to high water (HW). This deep intertidal morphology will create faster currents during the flood (flood dominant peak velocity) and encourage slower water movement around high water due to the deeper water over the intertidal areas (longer HW slack). In contrast, an intertidal area in which the average water depth is shallow (such as in the case of a convex-shaped depth profile) slows the progression of HW relative to LW, creating faster currents during the ebb (ebb dominant) and a shortened slack water period (shorter HW slack; Wang et al., 2002, Friedrichs, 2010).

The wetting and drying of intertidal areas further complicates patterns of tidal asymmetry in the upper reaches of an estuary. Due to a partially-progressive tidal wave (Hunt et al., 2015) and channelisation affects (Fagherrazzi et al., 2008), the timings of maximum ebb and flood current are delayed when the intertidal regions are shallow, and this delay results in maximum flood currents occurring when the upper intertidal is inundated and maximum ebb currents occurring when the water is constrained in the subtidal channel. This temporal asymmetry means that upper intertidal areas will always be flood dominant regardless of the dominance that may occur in the subtidal channel (Hunt et al., 2015). The effect of flood dominance on sediment deposition over the upper intertidal is strengthened when the duration of slack water at high tide is increased (which extends the time over which sediment can settle out of suspension over the intertidal areas).

Shear stresses created by wave orbital velocities are also highly influential in controlling sediment dynamics over intertidal areas (Green et al., 1997, Fagherazzi et al., 2006, French et al., 2008, Green, 2011) and have been cited as the main mechanism responsible for erosion on tidal flats (Fagherazzi and Wiberg, 2009). Waves create a suspended sediment gradient which can cause advection-driven sediment transport from areas of high to low concentrations (Jansen-Stelder, 2000) and also reduce the amount of time around slack water during which deposition can occur (Hunt et al., 2015).

Schematic modelling has provided support for the strong influence of waves on the shape and form of the intertidal morphology (Fagherazzi et al., 2006, Mariotti and Fagherazzi, 2013a, Hunt et al., 2015). When changes are forced by tidal processes alone, intertidal areas evolve towards a convex equilibrium shape (Roberts et al., 2000; Waeles et al., 2004, Friedrichs and Aubrey, 1996) in which the intertidal water depth is shallow relative to mean sea level (Fagherazzi et al., 2006, Mariotti and Fagherazzi, 2013a). Conversely, within wave dominated environments, the intertidal profile tends toward a concave shape in which the intertidal water depth is deeper relative to mean sea level (Friedrichs and Aubrey, 1996, Waeles et al., 2004, Bearman et al., 2010, Zhou et al., 2015). As the intertidal depth and extent is a principal control on the tidal asymmetry (Friedrichs, 2011), an understanding of estuarine morphological evolution will require that both waves and tides should be considered in combination (Mariotti and Fagherazzi, 2013a). In addition to generating short period waves, winds also strongly influence circulation patterns (Narváez and Valle-Levinson, 2008, Henderson and Mullarney, 2013) to the extent that they can influence the strength of tidal asymmetry (Hunt et al., 2015).

The research summarised above can be split into two categories: (i) detailed measurements of estuarine hydrodynamics over short (days to weeks) timescales and (ii) the theoretical longterm (decadal timescale) evolution of estuary morphology using models forced by wave and tidal processes. The ability of waves to shape the intertidal or the “morphological significance” of small waves in microtidal environments has been demonstrated previously (Green, 2011). Preliminary modelling work has shown that waves may also play a role in mesotidal estuaries (Hunt, 2015) where tides are normally considered to dominate and waves play a more minor role. Here, we extend on this work, and use a combination of hydrodynamic measurements and sediment deposition records to determine the conditions under which the observed waves are “morphologically significant” relative to tidal currents in a mesotidal estuary. Field measurements consisted of month-long hydrodynamic measurements of asymmetry and suspended sediment measurements, and were complemented by decadal-scale measurements of bed level, wind conditions, and comprehensive bathymetric information. Our measurements allow for the identification of the various spatial and temporal scales over which hydrodynamic processes operate. Waves are less predictable than tides, and although theory shows that waves can change asymmetries and play an enhanced role in driving morphological change relative to the more predictable tidal processes, such occurrences might be rare. Field measurements were collected in an estuary with two contrasting arms, one in which the dominant fetch is aligned to the typical wind direction and an arm that is not well aligned, and so we hypothesise that infilling will be prevented by waves for the fetch-aligned case, whereas tidal processes and accretion should dominate in the less aligned estuary.

2 Study area and field data collection

2.1 Study area

Raglan (Whaingaroa) Harbour is situated on the west coast of New Zealand's North Island (Figure 1a). The estuary is a flooded dendritic river valley and the mouth is partially enclosed by sand spits and dunes flanking the Tasman Sea. The estuary is mesotidal, with a spring tidal range of ~3 m (Sherwood and Nelson, 1979). Freshwater is supplied to the estuary from a number of tributaries of which the Waingaro and the Waitetuna are the largest. Total mean freshwater flow from all tributaries (18 m^3/s) is low compared to the tidal prism (46 x 10^6 m^3 and 29 x 10^6 m^3 during spring and neap tides, respectively) and therefore tidal processes dominate circulation within the harbour (Heath, 1976).

The dendritic form of Raglan estuary (Figure 1b) encompasses two distinct arms of the harbour connected by a confluence of the tidal drainage network; a 'fetch-aligned arm' (the Waingaro in the north) and a 'non-fetch-aligned' arm (the Waitetuna in the south) relative to the prevailing wind direction (Figure 2a). Wind speeds and directions recorded at Taharoa (situated on the open coast 40 km south of Raglan, Figure 1a) between 10th August 1978 and 1st January 2013 (Figure 1a) show that the prevailing northeast and southwest wind directions are aligned along the thalweg of the northern arm with stronger winds from the southwest (Figure 2a). Southwest winds are more frequent during the southern hemisphere summer (around December). The contrast between the two arms is clearly apparent when comparing the difference in occurrence of predicted wave height calculated using empirical equations from CERC (1984) with the fetch measured from aerial photography and the wind speeds and directions from Figure 2a (Figures 2b and 2c). Significant wave heights (H_s) in the southern arm (Figure 2c) are far lower and rarely exceed 0.3 m even during strong winds from the south west, whereas in the Northern arm, the same weather conditions create waves that exceed 0.5 m and occasionally reach 0.7 m in height (Figure 2b).

The bathymetry of Raglan Harbour was measured using LiDAR, bathymetry surveys (a combination of single beam and multibeam surveys) and the navigation chart (LINZ chart NZ4421). The bathymetry is summarised as hypsometric curves showing the dimensionless ratios of area against height for each arm of the harbour in Figure 1d. This comparison shows a distinct difference between the two arms of the harbour with the northern fetch-aligned arm (dashed line) exhibiting a slightly more concave form with deeper water levels over the intertidal flats (relative to MSL) and the sheltered southern arm (solid line) showing shallower water levels over the intertidal (relative to MSL) and a more convex intertidal shape. The contrast in the contemporary morphology between the two arms is also reflected in the records of morphological change from cores (Swales et al., 2005) and accretion plates. The southern arm has experienced sedimentation rates ranging from 0.35 mm/yr prior to human settlement increasing to 1.1 mm/yr since 1890 (following catchment deforestation), further increasing to 2.5 mm/yr since the early 1990s (Swales et al., 2005, Bentley et al., 2015) and ~ 3.4 mm/yr between 2003 and 2011. In direct contrast, the northern arm has experienced almost no contemporary sedimentation for at least the last 150 years (Swales et al., 2005), despite similar changes in catchment land-use. The texture of sediment data collected in Raglan Harbour also shows variability in the distribution of hydrodynamic energy, with the southern arm exhibiting a higher energy environment in the subtidal channels (coarser sediments) and lower energy environment on the top of the intertidal areas (finer sediments) (Sherwood and Nelson 1979). In the northern arm, the reverse is true, with textural patterns showing that often the higher intertidal flats are characterised by coarser sediments as indicative of higher energy environments (Sherwood and Nelson, 1979).

2.2 Instrumentation and methods

Field measurements were made within Raglan Harbour to examine if there was a contrast in the dominance of wave-induced relative to tide-induced dominance in asymmetry between the two arms (Table 1 and Figure 1). Currents and water levels in the northern and southern arms were recorded using a Sontek Acoustic Doppler Profiler (ADP) and Sontek Acoustic Doppler Velocimeter (ADV), respectively (Figures 1 and 3), between the 24th October 2012 and 20th November 2012. The ADV was deployed at the depth of low water (~3 m deep at high tide) at the interface between the intertidal flat and subtidal channel (Figure 1b) and wave data were also collected using the ADV pressure sensor.

The intertidal (water depth<2 m) hydrodynamics over the unfilled (northern) arm were recorded using instruments oriented along a ~200 m shore perpendicular transect (Figure 1b). This transect was first placed in an orientation perpendicular to the prevailing wind direction between 16th October and 7th November (T1) and then in an orientation parallel with the prevailing wind direction (T2) between 8th and 26th November 2012 (Figure 1b). The rationale behind this approach was to confirm predictions from idealised modelling of the conditions under which waves are the dominant control of bed-shear stress (Hunt et al., 2015). The instrumentation (Figure 1c) comprised an FSI current meter recording pressure and *u* and *v* components of the current, a DOBIE pressure sensor wave recorder and two co-located but vertically-separated OBS sensors mounted at the bed and ~0.4 m above the bed. Weather data (pressure, temperature, wind speed and direction) were collected between 30th April 2012 and 29th September 2013 and the measurements overlapped the hydrodynamic deployments.

The DOBIE and ADV pressure data were corrected for atmospheric pressure (recorded by the weather station) and converted to hydrostatic depth assuming a representative seawater density of 1018 kg/m^3. The surface wave spectrum was then reconstructed from each wave burst. To correct for the attenuation of higher frequency waves, wave spectra were extrapolated to estimate the energy above the cutoff frequency using an f^{-4} curve, a technique which has successfully been used in similar estuarine environments (e.g. Smith et al., 2001, Jones and Monismith, 2007, Mariotti and Fagherazzi, 2013b). All spectra were truncated and extrapolated at a fixed frequency cutoff of 0.8 Hz through to 5 Hz for the DOBIE and 2 Hz for the ADV (the Nyquist frequency of each instrument). Significant wave height and peak and mean period were then calculated from the spectral moments. Finally, all waves with a H_s of less than 0.05 m were discarded to allow for any potential errors associated with pressure measurements and the analysis (e.g. following Mariotti and Fagherazzi, 2013b).

Bed shear stress due to currents (τ) was calculated using the recorded tidal current speeds and water depths in the equations described in Soulsby (1997) and

Whitehouse et al., (2000). For the depth averaged velocities recorded by the ADP, τ was calculated as

$$\tau = \rho C_D \overline{U}^2, \tag{1}$$

where the drag coefficient (C_D) is

$$C_D = \left[\frac{0.40}{1 + \ln z_0/h}\right]^2, \tag{2}$$

where z_0 is the bed roughness length, h is water depth, ρ is density of water and $\overline{U}$ is depth averaged current speed.

For the ADV and the FSI current meter, τ is calculated using current speed at a fixed depth using

$$\tau = \rho {u_*}^2, \tag{3}$$

where u_* is the friction velocity

$$u_* = U \times 0.40/\ln\left(\frac{z}{z_0}\right), \tag{4}$$

in which U is the horizontal component of water velocity at height z above the seabed. z_o is the bed roughness length, which although not measured directly, was chosen using the measured values reported in Soulsby (1997), for the seabed sediment type that was observed at the site.

Bed shear stresses due to the effect of waves alone (τ_w) were calculated using the recorded significant wave height (H_s) and wave period (T) and the following equations (Soulsby, 1997 and Whitehouse et al., 2000):

$$\tau_w = \frac{1}{2}\rho f_w U_w^2, \tag{5}$$

where the wave orbital velocity amplitude at the seabed, U_w is

$$U_w = \frac{\pi H_s}{T \sinh kh}, \tag{6}$$

and where κ is the wave number and the wave friction factor (f_w) is the larger of either the rough-bed wave friction factor (f_{wr}) or the smooth-bed wave friction factor (f_{ws}) (Soulsby, 1997), i.e.

$$f_{wr} = 1.39\left(\frac{A}{z_0}\right)^{-0.52}, \tag{7}$$

$$\text{or} \qquad f_{ws} = BR_w^{-N}. \tag{8}$$

The coefficients B and N were selected based on the wave Reynolds number as recommended by Soulsby (1997),

$$R_w = \frac{U_w A}{v}, \tag{9}$$

where v is the kinematic viscosity of water and the orbital amplitude of wave motion at the bed (A) is given by

$$A = U_w T/2\pi. \tag{10}$$

For $R_w \leq 5 \times 10^5$, $B = 2$, $N = 0.5$ (laminar flow) and for $R_w > 5 \times 10^5$ $B = 0.0521$, and $N = 0.187$ (smoothly turbulent flow).

Finally, bed shear stresses due to tides and currents combined (τ_{max}) were also evaluated using methods described in Soulsby (1997) and Whitehouse et al., (2000):

$$\tau_{max} = [(\tau_m + \tau_w \cos\phi)^2 (\tau_w \sin\phi)^2]^{1/2}, \tag{11}$$

in which

$$\tau_m = \tau\left[1 + 1.2\left(\frac{\tau_w}{\tau+\tau_w}\right)^{3.2}\right] \quad , \tag{12}$$

where τ_m is the mean bed shear stress during a wave cycle under combined waves and currents, and ϕ is the angle between current direction and direction of wave travel. Wave data from the DOBIE pressure sensor is non-directional and therefore wave travel direction was assumed to be the same as the wind-direction recorded at the Raglan weather station situated <10 km from the DOBIE pressure sensors

(Figure 1b). Waves refract as they propagate over intertidal flats. To test whether the use of wind direction is suitable as a proxy for intertidal wave direction, a SWAN-Delft3D model was run, calibrated using the data collected here. The mean difference between τ_{max} calculated from the model and τ_{max} used here differ on average by only 0.0384 N/m^2 at Transect 1 and 0.0259 N/m^2 at Transect 2. Moreover, linear regression comparing the two calculated timeseries of τ_{max} shows good agreement between the two methods at both Transect 1 (r2 = 0.99 and RMSE = 0.065 N/m^2) and Transect 2 (r2 = 0.96 and RMSE = 0.050 N/m^2).

3 Results

The data recorded by the instruments are summarised in Figure 3. The tidal stage diagrams for τ are shown in Figure 4, which compares the magnitude and duration of τ through the ebb stage (negative τ values) and flood stage (positive τ values) of the tide highlighting the timing, strength and direction of tidal asymmetry. The tidal stage plots for the northern part of the estuary exhibit no clear tidal asymmetry in the subtidal channel (Figure 4a, solid blue line) with only a very weak dominance during the ebbing part of the tide at a water level of 3 m. This pattern of tidal asymmetry would result in no net direction of sediment transport with almost equal τ during the flood and ebb. However, during the intertidal T1 deployment (location on Figure 1b) the τ (Figure 4a, dotted line) indicate flood dominance on average with higher maximum τ occurring during the flood stage of the tide. The deeper T2 deployment (Figure 4a, dashed line) also shows a clear pattern of strong flood dominance with a marked strengthening of the τ maximum during the flood tide; this flood dominance tends to strengthen during springs and weaken during neaps (not shown).

The difference in tidal asymmetry between the subtidal and intertidal areas occurs due to a temporal asymmetry between the timing of maximum ebb and maximum flood flow, which is evident in measurements from the T2 deployment (Figure 4a dashed line), in which the flood maximum occurs when the water level is at 2.8 m and the ebb maximum occurs when the water level is at 2.4 m. Overall these asymmetries cause the maximum flood current to occur when the water occupies the intertidal area and the maximum ebb to occur when the water is below the intertidal surface. Therefore flood-dominant asymmetry always occurs over the shallow intertidal areas in this situation regardless of the relative strengths of the maximum flood and ebb velocities in the subtidal channels. The subtidal deployments in the northern and southern arm show a strong rectilinear tidal pattern that is parallel with the orientation of the subtidal channel. In contrast the intertidal currents are less rectilinear but in general exhibit a cross shore orientation at T2 and an alongshore orientation at T1.

In the absence of waves, the tidal currents clearly control the pattern and strength of suspended sediment concentrations with higher concentrations occurring during the flood stage of the tide (Figure 5a and 5b). The suspended sediment concentration decreases during slack water when sediment can fall out of suspension and deposit on the seabed. Following high tide, the suspended sediment level increases again during the ebb but by a lower magnitude than that during the flood (Figure 5b) resulting in a net sediment flux in the landward direction. This net landward transport of sediment is contrary to the lack of accretion in the sediment records.

The southern sheltered arm of the harbour shows a clear trend of ebb dominance with stronger currents during the ebb phase of the tide (Figure 4b). The ebb dominant hydrodynamics in the subtidal area of the southern arm should indicate a system that exports sediment; however, sediment plate data and sediment cores of historical deposition indicate an accretional regime (Swales et al., 2005). Velocity data from the southern arm show a marked temporal asymmetry with the timing of maximum velocity delayed during both the flood and ebb stages of the tide. This delay means that the maximum flood velocity (and τ) occurs closer to high water and the upper part of the intertidal area (>~2 m above LW) will be flood dominant whilst subtidal currents remain ebb dominant.

The observed wave heights H_s at transects T1 and T2 can be clearly related to the fetch at each location. Figure 6a shows the recorded significant wave height from the DOBIE pressure sensor and the corresponding wind direction recorded at the Raglan weather station during the T1 and T2 deployments. Figure 6b shows wind directions and speeds during the T1 and T2 deployments recorded at the Raglan weather station. During the T1 deployment, the largest waves occur with winds from the SWW to the NW sectors (Figure 6a); this direction coincides with the strong winds from these sectors but not directly with the prevailing winds from the SW (Figure 6b) due to the sheltering effect of the peninsula to the west of the deployment (Figure 1b). At T2, the largest waves occur during the prevailing winds from the SW due to the large fetch exposure from this direction. The largest H_s occurs at T2 despite the lower wind speeds measured during this deployment, due to the exposure at T2 to the largest fetch direction (which is also the prevailing wind direction).

Three tidal cycles were selected to illustrate how the patterns of bed shear stress and suspended sediments are modified during wave events (Figures 5c – h) compared to the previously described tide-only (H_s < 0.05 m). During wave events (Figures 5c – h), the flood-directed suspended sediment flux on the intertidal that occurred when tidal processes dominated (Figures 5a and b) is reversed by the increase in suspended sediment concentrations both during the ebb stage of the tide and during slack water. For example, during a wind speed of 5.7 m/s from 246° during a spring tide, τ_w progressively increased throughout the tidal cycle due to a lengthening fetch with the incoming tide (Figure 5c). Measurements from aerial photography show that the potential fetch from this wind sector is 3.74 km at HW. Maximum τ_w occurs during the ebb stage of the tide as a result of a balance between fetch length and the amount of time over which the wind has been blowing over this fetch. This modified pattern of bed shear stress prevents deposition at high water creating a greater flux of sediment during the ebb tide. During a higher wind speed (7.6 m/s) over a similar wind direction (258°), the fetch length (3.56 km at HW) becomes less important and so τ_{w} and τ_{max} increase rapidly during the flooding tide (Figure 5e) and the large suspended sediment concentrations at high water (Figure 5f) show that wave conditions completely halt any deposition that would have occurred during slack water. During neap tides (Figures 5g and h), a lower wind speed (4.6 m/s) from 246° creates a similar pattern of peak suspended sediment concentration to that in Figures 5e and 5f, albeit of a lower magnitude. The marked reduction in slack water duration observed during these scenarios is due to reduced attenuation of orbital velocities in shallower waters, meaning that shallow water depths are sensitive to frequent, smaller waves that inhibit sediment deposition around high water. Although no suspended sediment data were available for the T1 deployment, the patterns of τ , τ_{w} and $\tau_{\max}$ (Figure 7) support those shown by the T2 deployment (Figure 5) for both larger wave events (Figure 7c) and smaller wave events during both a spring (Figure 7b) and a neap tide (Figure 7c).

Analysis of the wave data showed that the wave climate at site T1 was more susceptible to changes in wind direction than at site T2. This heightened sensitivity of waves to wind at site T1 results from the site's exposure to different combinations of fetch length and wind direction (Figure 1a). In contrast, T2 is generally exposed to the largest overall fetch length that remains coincident and aligned with the prevailing wind direction. This result implies that the region most affected by waves (in terms of sediment movement or 'geomorphological significance') may not be the region with the longest fetch (and therefore the largest waves) but is the region with the most exposure to a range of fetches that generates waves with sufficent energy to mobilise sediment. So, although T2 experienced higher H_s, T1 had higher τ_w, which can be attributed to the shallower water depths at T1 and resultant reduced attenuation of orbital velocities (Figure 1e).

The influence of wind on general circulation patterns can also be seen at the T2 deployment where a wind from the west (blowing up-estuary) reduces τ during the flood and increases τ during the ebb (Figure 5e). To identify the significance of any links between tidal asymmetry and wind circulation, the strength of tidal asymmetry (defined here as the ratio between mean ebb and mean flood current speeds) was compared to wind strength. This comparison shows, a correlation at the T2 (r^2 = 0.50, F = 25.69, p < 0.01) deployment, a weak correlation in the ADP observations (r^2 = 0.05, F = 3.06, p = 0.09) and no correlation during the other deployments. As the higher wind speeds are associated with the fetch aligned winds from the SW and W (Figure 2a), the wind driven current should weaken flood currents and / or strengthen ebb currents at the T2 and ADP deployment site. These results indicate that wind-driven circulation is most important over the downwind intertidal areas of the estuarine system.

Within the southern arm, the ADV did not record any waves higher than 0.06 m; most waves (99.5% of the record) were below the significance threshold of 0.05 m meaning that the majority of the record is indistinguishable from the errors introduced in this type of analysis. Therefore any waves within the southern arm of the estuary were too small to be characterised accurately by the ADV. In addition to the small size of measured waves, there was almost no correlation between the wave size and the wind speed or wind direction. The small wave height and lack of correlation with the wind is attributed to the short fetch distance available in any direction for wave generation when compared to the longer and straighter northern arm (Figure 2c).

In summary, the flood dominant tidal asymmetry over the intertidal northern arm does not explain the lack of recorded deposition in the sediment plate and sediment cores. Instead the waves have been observed to reverse the flood dominance in shear stress asymmetry, provided that the water levels are shallow enough and the fetch axis coincides with the prevailing wind direction. The distribution of bed shear stress and suspended sediment concentration shows landward sediment flux (accretion) when driven by tides alone, and seaward sediment flux (erosion) when waves and tides occur together. In the sheltered southern arm, no waves were recorded and the historical accretion is likely to be due to the tidally-dominated environment since the timing of maximum velocities makes ebb dominance over intertidal areas unlikely regardless of the strength of the ebb tidal current within the subtidal channel.

4 Discussion

4.1 Contrasting pathways to equilibrium in the two arms

Absolute long-term morphological stability or “stationarity” (Woodroffe, 2002) is unlikely in any estuary because the hydrodynamic and sedimentological processes that control the pathway to equilibrium are themselves not stable over long timescales. Instead a dynamic equilibrium exists and the perception of stability will depend on the timescale considered. Stable estuarine morphology over a >10 year and <100 year timescale is critical for the development of habitats such as mudflats, mangroves, saltmarsh, seagrass and shellfish beds with the shape of the stable-form being dependent on the hydrodynamics, sediment supply and any non-linear interactions between these variables (McGlathery et al., 2013). The analysis of hydrodynamic and sedimentological records supports the existence of two alternative pathways to morphological equilibrium within the different arms of a mesotidal, dendritic estuarine system (Whangaraoa Harbour, in New Zealand). Most importantly, the difference in the tidal asymmetry between these two arms does not explain the observed differences in patterns of erosion and accretion. Instead, this work shows that this difference is due to the prevailing wind direction relative to the estuarine morphology, and alignment of the longest fetch. Waves generated on a fetch-aligned morphology promote erosion of intertidal sediments.

Prior research has predicted the net tidal asymmetry (and consequently the pathway to establishing a stable shape) within an estuary from the geomorphological parameters that describe the basin (Friedrichs and Aubrey, 1988, Dronkers, 1986). This approach is advantageous as it allows the quick classification of an estuarine system without detailed hydrodynamic measurements or numerical modelling. However, the analysis in this study shows that the direction of tidal asymmetry and sediment flux can be highly variable throughout an estuary. Therefore, the tidal asymmetry recorded within the main channel does not necessarily provide insight into patterns of erosion and accretion over the intertidal. This result is supported by previous numerical modelling studies of idealised estuarine environments (Robins and Davies, 2010, Hunt et al., 2015). The intertidal areas can form a large proportion of an estuarine basin and therefore are a critical consideration when determining if an estuary is a net source or sink for sediments. For example, ebb-dominant channel asymmetry could indicate that the estuary is exporting sediment as a whole, or it could indicate that the estuary is developing channel networks where the tidal channels are eroding at the same time as the tidal flats are infilling This discrepancy between intertidal and subtidal processes, the spatial variability in tidal asymmetry and the critical role that waves play, can result in the use of a single descriptor of tidal asymmetry for an entire estuary being misleading.

The empirical evidence from this study demonstrates that when conditions are dominated by tidal processes (such as in the southern arm), accretion over the intertidal areas continues despite ebb-dominance in the subtidal channel. We show that accretion is likely to be a direct consequence of the flood dominance that occurs when the intertidal area is inundated at high tide, directing the net flux of sediment landward with settling of sediment on the intertidal during high tide slack water. Flood dominance over the intertidal occurs due to a delay in the onset of maximum flow and can arise if a tidal wave is partly progressive and the timing of the current maxima and water level maximum are somewhere between in phase and in quadrature (Bowers and Al-Barakati, 1997, Hunt et al., 2015). The timing in the onset of the maxima in ebb and flood velocity (and τ) is also affected by channelisation and the delay in the propagation of the tidal signal within the intertidal area (Fagherazzi et al., 2008). Modelling using a series of idealised estuarine basins showed how increased sediment infilling and reduced water depths over the intertidal areas of an estuary enhances this intertidal flood dominance (Hunt et al., 2015). Hence, in the cases where flood-dominant intertidal occurs, there is no evidence of erosion in the basin as a whole caused solely by the influence of the tide. When there is no net export of sediments from the tidal flats, intertidal stability can only be reached through infilling to a point where either tidal currents are too weak to transport sediments further landward or when mangroves and saltmarshes stabilise the intertidal regions at a species-favourable elevation. The high intertidal areas enhance ebb-dominance in the incised subtidal main channel; this ebb dominance would flush any sediment not deposited on the intertidal out into the adjacent estuary and open coast (van Maanen et al., 2013a). This morphological form is similar to that proposed by Mariotti and Fagherazzi (2013a) and to the convex-up estuary form proposed by previous researchers (Roberts et al., 2000; Waeles et al., 2004, Friedrichs and Aubrey, 1996; Friedrichs, 2011, Kirby, 2000; Kirby, 2002; Mehta, 2002; Bearman et al., 2010, Zhou et al., 2015).

In contrast, the wave-dominated environment (northern arm) shows continued periodic erosion despite stronger tidal currents during the flood stage of the tide. In this case, stability is likely to be reached when opposing forces of erosion (from waves) and accretion (from tides during calm periods) balance to form an intertidal area over which the water is deeper relative to the tidally dominated environment. Erosion from waves occurs due to a reduction in the time during which water is slack at high tide (preventing deposition) and an increase in suspended sediment concentrations over the intertidal area relative to the channels, thus creating a seaward gradient in sediment flux. Idealised modelling in a series of basins with the same fetch as the northern arm but with varied amounts of intertidal sediment infilling shows that the reduction in slack water at high tide and the increase in average bedshear stress over the intertidal relative to the subtidal are augmented with larger amounts of intertidal infilling (Hunt et al., 2015). The contrast in patterns of SSC observed here between spring and neap tides also show that attenuation of orbital velocities with water depth is rapid and very sensitive to subtle changes in depth. The depth at which the intertidal flat stabilises will theoretically be around the depth where the most common wave event attenuates at high water. This wave attenuation allows the deposition of sediment during slack water; the resulting deposition reduces the water depth. When the water becomes shallower, the wave orbital velocities can more easily reach the bottom, thus halting deposition, causing erosion and returning the bed to a lower elevation. Thus, there exists a stable elevation which is determined by a subtle balance between the estuarine fetch and average wind strength (Fagherazzi et al., 2007).

The contrast in intertidal morphology and hydrodynamics between the two instrument transects indicates that increased concavity of the intertidal profile results in reduced erosion and therefore is the stable profile that evolves under the influence of wave processes. The morphology of the northern arm has been summarised as a hypsometric curve (Figure 1d) but a comparison of the intertidal profile collected along each instrument transect (Figure 1e) shows local morphological variation and a clear contrast between the shape of the two profiles where measurements were collected. At transect T1, the intertidal slope is linear whereas at T2 the slope is more concave in shape; this greater concavity at T2 is in indicative of the greater wave exposure at this site. The concave profile at T2 results in a deeper intertidal compared to the profile shape at T1; this greater water depth considerably reduces τ_w and τ_{max} due to the increased attenuation of wave orbital velocities (Figures 5 and 7). However, the bed substrate may also contribute to the intertidal shape with T2 being more readily erodible and T1 featuring patches of exposed rock platform and oyster beds.

Modelling of the evolution of idealised funnel-shaped estuarine morphology (Lanzoni and Seminara, 2002) has shown that long-term intertidal stability is reached through estuarine infilling to the point at which no tidal sediment transport is possible as opposed to a switch from flood to ebb dominance (‘dynamic equilibrium’) as theorised elsewhere (e.g. Pethick, 1994, Friedrichs, 2010). Instead, our observations show that the main hydrodynamic mechanism for controlling the switch between infilled and unfilled intertidal morphologies is provided by short period wind waves (as suggested by Mariotti and Fagherazzi, 2013a). Consequently the amount of sediment infilling over intertidal areas is better explained by the frequency and magnitude of wave generation, with tidally dominated intertidal environments tending to be shallow and accretional and wave dominated intertidal environments tending to be deeper and erosional. Therefore, perhaps somewhat counter intuitively, stochastic wave and wind processes control the intertidal form of the estuary rather than the strength of tidal forcing. Overall, the evidence from this study shows two contrasting pathways to stability in estuarine systems, one in which tides create a stable intertidal morphology through accretion and infilling, and another in which waves create a stable intertidal morphology through opposing processes of erosion (from waves) and accretion (from tides). The ability of waves to maintain this stable equilibrium will also be influenced by sediment supply (Fagherazzi et al., 2006 and Fagherazzi et al., 2007) and in regions with an exceptionally large sediment supply such as the Suriname Coast between the Amazon and Orinoco Rivers, accretion has been recorded despite the erosive affects of wave action (Wells and Coleman, 1981, Augustinus, 1980).

4.2 Timescale of processes

The hydrodynamic processes recorded in this research operate over a range of temporal scales. The cumulative temporal effect of these processes is to drive the pathway to a presumed dynamic equilibrium which is different in the two arms of the harbour. A comparison of the timescales over which each hydrodynamic process operates shows a range from frequent, accretional low magnitude changes through to infrequent, erosional high magnitude changes (Table 2). Tides are the most regular of these timescales, creating hydrodynamic process that operate on a semi-diurnal frequency. The tidal asymmetries recorded here suspend less sediment than waves but because they are regular, have been shown by models to become morphologically significant over a long timescale (Lanzoni and Seminara, 2002).

Normally wave conditions are considered to be episodic, but here there is evidence of a consistent daily sea-breeze (~5 m/s) (Figure 3e and Figure 8) whose effect on intertidal sediment suspension will depend on whether the maximum sea breeze coincides with the maximum fetch-depth conditions that maximise wave bed shear stress. Thus, the stable intertidal depth that occurs in fetch-aligned estuaries will be modulated by the interaction between the sea-breeze and the spring-neap cycles. Proportionally, these moderate daily wind events tend to have a greater morphological impact than tides because although they are slightly less frequent, wave action stirs up more sediments than tides alone. The stage of the tidal cycle with which the wind coincides is critical to determine the modification of SSC patterns due to τ_{max}, especially over the intertidal areas, a factor which is often neglected in numerical modelling studies which tend to use a constant breeze over the tidal cycle (e.g. Talke and Stacey, 2008). The size of the waves generated within an enclosed body of water is dependent on the interplay between the fetch and the wind speed. With higher wind speeds, fetch becomes a less critical factor in generating waves (Mariotti and Fagherazzi, 2013b) and waves capable of moving sediment could theoretically be created over even small fetches. During this observation period, only wind events with a speed~<10 m/s) were observed and so the potential for wave generation during stronger wind events could not be examined. A higher wind speed (>10 m/s) may be capable of generating waves even in the sheltered southern arm of the harbour; however, such an event would be infrequent (during only 0.002% of the long term record) and therefore presumably of low morphological significance. Moreover, infrequent wave events in the southern arm of the harbour could allow the growth of biofilms on the intertidal areas between wave events which can further stabilise the intertidal flats (Mariotti and Fagherazzi, 2012b).

Studies of estuarine environments using field observations and analytical models have shown that local winds create a superimposed residual current (Wong, 1994, Sanay and Valle-Levinson, 2005; Narváez and Valle-Levinson, 2008, Hunt et al., 2015). In the shallow areas adjacent to the main channel, the acceleration from wind drift increases the flow in the same direction as the wind raising the water level downwind and forming a pressure gradient. This pressure gradient returns water against the wind down the channel resulting in a flow that opposes the wind (Wong, 1994; Sanay and Valle-Levinson, 2005; Narváez and Valle-Levinson, 2008, Hunt et al., 2015). When modelled in a series of elliptical idealised basins with a similar fetch to the northern arm the current circulation patterns caused by changes in wind direction relative to the estuaries orientation were more apparent than recorded here and strengthened or weakened currents over the intertidal and subtidal either side of a stable node (Hunt et al., 2015). Here, the correlation between wind speed and current velocities is not strong, probably because the variability in current speeds depend on the patterns of wind speed and direction but will also depend on spring and neap cycles and the timing of the wetting and drying of morphology around intertidal features such as mussel and oyster beds which are located throughout the fetch aligned (northern) arm of the harbour.

4.3 Defining morphologically-active wind conditions

The wind speed threshold at which waves entrain sediment on the intertidal to a greater extent than in the channels (causing a seaward gradient in sediment flux) can be considered to be the point at which waves become “morphologically significant” and can be inferred by comparing τ in the subtidal channel (ADCP) to τ_w over the intertidal areas (T2 and T1). When $\tau_w > \tau$, more sediment will be in suspension over the intertidal areas and the advection gradient will be seaward. Furthermore, an increased value of τ_w during slack water will inhibit the deposition of sediments over the intertidal areas. For example, when tidal processes dominate and τ (channel) > τ_w (intertidal) (Figure 5a and 5b), there are higher concentrations of suspended sediment during the flood tide compared to the ebb. The higher concentrations are partly due to local resuspension by the stronger flood tide and partly due to suspended sediments advected into the study area from the more energetic subtidal channel and the lower intertidal flats following the turbid tidal edge (Mariotti and Fagherazzi, 2012a). In this scenario, suspended sediment is brought onto the intertidal flats during the flood tide and deposited during slack (high) water. This sediment transport process is the effect that is known as settling lag, and is associated with the landward fining of sediments that is common in many estuaries (Zhou et al., 2015). When waves are included and τ (channel) > τ_w (intertidal), suspended sediment levels are greater over the more energetic intertidal flats and therefore more sediment is transported seaward during the ebb stage of the tide (Figures 5d, 5f and 5h). Waves also shorten slack water preventing the usual deposition of sediments at high water (Figures 5d, 5f and 5h).

Although waves reduce the period of slack water duration and therefore inhibit the deposition of sediments, it is known that wave dissipation can also occur causing sediment to fall out of suspension. However, wave dissipation is restricted to the shallowest parts of the intertidal flats (Green, 2011) and therefore the degree to which fine sediment can accumulate in the upper intertidal in a wave dominated environment depends on the shape of the intertidal and how much space there is between the turbid fringe and the shoreline. If this area is small, it is inundated for such a short time that the sediments do not have a chance to fall out of suspension. When the estuary basin is wave dominated and more concave (such as in the northern arm of the study site) the shallower areas where dissipation is likely cover a smaller proportion of the basin and therefore the possibility of fine sediment accumulation under waves is only small over a wave dominated concave intertidal area. Furthermore, dissipation over the shallow upper intertidal areas will only occur once waves reach a certain size. Smaller waves that will form regularly under even low wind speeds have been shown to be effective at eroding bed sediments even over these shallow areas (Green, 2011) and therefore the shallow areas of a wave dominated environment cannot be considered as exclusively depositional.

Although it is difficult to pinpoint the precise wind threshold at which the change from landward to seaward flux occurs owing to the limited number of wind events recorded here (typically <10 m/s), we can estimate this threshold by calculating H_s, Tp and τ_w for wind speeds ranging between 1 and 15 m/s using empirically based equations (CERC, 1984 and Soulsby, 1997). The intertidal profile and variability in fetch length (maximum of 5 km) used in this calculation was based on transect T2 (Figure 1b and 9b) and the water levels and τ were taken directly from the ADCP.

Three representative events were chosen based on a neap (Figure 9e), a spring (Figure 9d) and an intermediate tidal cycle (Figure 9c). Significant wave heights less than 0.05 m and water depths of less than 0.1 m were removed from the calculations so the results could be compared directly to those recorded by the DOBIE wave gauge (Figure 9a). These calculations do not consider the contribution of intertidal currents (i.e. τ_w only as opposed to τ_{max}), which is a robust assumption for the purposes of this experiment as τ_w was found to contribute the greatest proportion of τ_{max} during the field deployment (Figures 5 and 7).

The majority of the intertidal flat experiences a reversal of the advection gradient between the intertidal and the channel when wind speeds reach ~ 10 m/s regardless of the tidal state (Figure 9a), thus defining a wind threshold for 'morphologically-active' conditions. This threshold varies during either spring or neap tidal conditions due to the relative strength of τ in the channel. A partial reversal, with $\tau_w > \tau$ around slack water is also possible, with ~ 5 m/s required to initiate a noticeable increase in τ_w (Figures 9a, c, d and e) relative to τ. Over the deeper parts of the intertidal profile, a wind event that creates a partial reversal (at slack water) during an intermediate tide (Figure 9c, when the solid light blue line is greater than the solid thick black line) may create an almost complete reversal if it occurs during neap tides when current speeds in the subtidal channel and water depths over the intertidal are low (Figure 9e, compare solid light blue line and solid thick black line). A complete reversal of the sediment gradient is predicted during a wind speed of 5 m/s for all tidal states at the shallower end of the profile (Figures 9c, d and e, dashed lines), because the orbital velocities are readily able to reach the seabed. This pattern of greater levels of τ_w over the shallower areas indicates that the upper part of the intertidal will be prone to more frequent erosion even during the weaker wind events. Overall, when winds are weak (~5 m/s) the reduction in sediment deposition is controlled primarily by water depth and the timing of the wind event relative to the spring – neap tidal cycle. When winds are stronger (>10 m/s) the depth or tidal state are no longer an important control and erosion will occur throughout the intertidal profile.

To explore the dependence of the morphologically significant wind conditions on fetch length, the calculation is now repeated for an estuary with the same intertidal profile and wind conditions but a shorter maximum fetch of 2 km (Figure 10). This fetch length is similar to the maximum fetch length in the southern arm of the study site. The shorter fetch results in a dramatic reduction of τ_w for all water depths, tidal states and wind speeds, with a stronger wind speed required to create the comparable level of τ_w calculated within the estuary with the longer fetch. The reduction in τ_w is especially apparent for the deeper parts of the intertidal profile which rarely exceed the τ within the main channel (Figures 10c, d and e, solid and dotted coloured lines). In this reduced fetch scenario, the deeper parts of the intertidal are rarely disturbed by wave action (low τ_w) and will infill until a shallower depth is reached at which erosion is initiated by waves (high τ_w). This shallowing of the lower intertidal would change the profile from concave to more convex as is observed in the southern arm of the case study site. The generation of small waves capable of increasing τ_w over the shallower intertidal areas is less limited by fetch length; especially at wind speeds > 10 m/s (compare τ_w for dashed lines in Figures 9c, d, and e with 10c, d and e). Therefore, these waves will theoretically only become “morphologically significant” over the shallow upper intertidal in any estuary independent of the fetch length, or the prevailing wind direction relative to the fetch, when winds exceed 10 m/s.

Previous research has identified links between coastal morphology and the wind climate which is in turn related to the strength of El Niño and La Niña events (e.g. Ranasinghe et al., 2004). Here, sedimentary and climate records were analysed to identify any similar trends of morphological variability in an estuarine environment. If the sediment processes in the contrasting arms of the harbour (Figure 1) depend on the differing exposure to wind, then the bed level records in the fetch aligned northern arm should show a long-term correlation with variability in wind direction and speed whereas the bed levels in the southern arm will not. To analyse the longer term climate patterns, records of wind direction and speed covering the bed level measuring period where obtained for the Taharoa weather station from NIWA and the Oceanic Niño Index was obtained from NOAA. The Oceanic Niño Index (ONI) shows the strength of either an El Niño (warm) or La Niña (cool) event in the tropical Pacific using a three-month running-average of the sea temperature anomaly. NOAA define an El Niño event as when the temperature anomaly exceeds 0.5° C and a La Niña event when the anomaly falls below -0.5° C. The Taharoa wind data (long record) was modified using Raglan (short record) by determining the fit of the U and V components where the data coincided and applying this fit to the rest of the Taharoa record. The wave generation criteria is based on the wave, wind and suspended sediment data obtained during the fieldwork period and is defined as a wind direction between 180 and 270° (also the longest fetch distance in the northern arm), these events were then binned according to speed and expressed as a percentage of all the records taken during each proceeding 3-month window.

The wind record (Figure 11a) shows that south westerly winds are at their most frequent (dark blue line) during the summer season and at their least frequent during the winter season. The strength of the El Niño / La Niña cycle from the ONI (Figure 11a, black line) shows that there is a pattern between the strength of the ONI and the frequency of south westerly winds with a strong El Niño event during December increasing the frequency of winds from the sector between 180 and 270° by ~10-20 % ($r^2 = 0.52$, $F = 19.47$, $p < 0.01$). The seasonality in SW winds and the correlation with the ONI during the summer is only apparent when considering bins that include the lower wind speeds (> 1, > 2, > 3 and > 4 m/s). When the morphologically significant wind threshold is exceeded (> 5 m/s, Figure 11a, green line) there is no correlation between ONI and wind frequency and no seasonal signal, instead the occurrence of these wind speeds is relatively consistent throughout the record. Winds > 8 m/s are extremely rare ranging between 0 and 6.5 % of the record. Overall the winds between ~5 - 8 m/s are critical as they are not only morphologically significant in the fetch aligned arm (Figure 9) but are frequent and consistent enough to generate waves over a regular and non-seasonal scale. At these wind speeds the tidal stage is extremely important due to the magnitude of τ in the subtidal channel and the depth over the intertidal flats, with more erosion during neaps and more accretion during springs (Figure 9a).

Although some seasonality is apparent within the sediment record at Whatitirinui Island (Figure 11b) where the bed level tends to drop in the winter and rise in the summer, it was not possible to statistically correlate the south westerly wind frequency and the magnitude of bed change with an acceptable level of significance or confidence due to the poor temporal resolution of the bed-level dataset and the lack of seasonality of morphologically significant (> 5 m/s) winds. The bed level records show two distinct sedimentary environments with the southern tidally dominated arm (Figure 1b) progressively infilling with limited periods of erosion. This sedimentation pattern is indicative of gradual sedimentation during slack water, interspersed with erosion from rare wave events during storms where wind speeds are strong enough to overcome the limited fetch. The accretion rate recorded over the sediment plates ranged between 2.4 and 5.3 mm/year with an average of 3.39 mm/year; these rates are close to the long term estimate from sediment cores which estimated 2.5 mm/year since the early 1990s (Swales et al., 2005, Bentley et al., 2014). In contrast, the bed levels within the exposed part of the northern arm are more variable over time but less variable between the plates, with periods of erosion followed by accretion and a net trend of stability or erosion overall. This pattern is indicative of a stochastic or seasonal process, with periods of deposition (tides only) followed by periods of erosion (waves) which depend on the overall wind climate. Previous research in microtidal environments has also demonstrated the morphological significance of frequent small waves compared to occasional storm events where tidal processes are considered to be negligible (Green, 2011). Here we show that waves can also be morphologically significant in mesotidal systems but most importantly that the interactions between wind, tides and waves are of crucial importance when defining this significance within these environments.

Often attempts are made to predict the future morphology of estuaries using a calibrated hydrodynamic process-based numerical model focusing predominantly on the predictable and repeatable pattern of tides. Future changes in sea level from ice melt and thermal expansion can be incorporated into such models by adjusting the tide by the amount predicted by global climate change models (van Maanen et al., 2013b, van Maanen et al., 2015) and relative sea level rise can be accounted for by using the projected local rate of subsidence or uplift based on geological and GPS records. However, the analysis presented here demonstrates that the estuary morphology is also highly sensitive to the wave climate to the extent that the observed morphological change can be better explained by waves rather than tides and therefore waves need to be considered in predictions of long-term morphology in estuaries. Overall, waves can be considered as a "morphologically significant" process where the prevailing wind direction is oriented to create a sufficient fetch to generate waves under frequently occurring wind speeds.

5 Conclusions

The aim of this research has been to investigate the relative morphological significance of tidal, wind and wave processes in a meso-tidal estuary using a combination of sedimentological, hydrodynamic and climatic records. The threshold of this morphological significance depends on a combination of magnitude and frequency whereby the generated waves can influence tidal and suspended sediment flux asymmetry on a regular enough basis to control the subsequent infilling over longer timescales. Here, we have shown that waves occur due to winds operating over two distinct timescales, daily (sea breeze) and episodic (storms) and the fetch length is critical when considering the magnitude of morphological response to these wind events. Overall, waves are shown to be more morphologically significant in areas with longer fetches because weaker, more frequent daily winds can generate waves. Conversely the morphological significance over shorter fetch lengths depends on the less frequent perturbations caused by storm events. In the absence of waves, tides invariably cause accretion due to flood dominant currents and deposition around slack water. Therefore, fetch limited systems will accrete except during storm events when wave size is not fetch limited. Water depth is also a critical control on sedimentation, as the short-period waves generated within estuaries are attenuated rapidly with increasing water depth and this water depth varies throughout the spring-neap cycle. Therefore, morphologically significant wave conditions occur under weaker winds in the shallower parts of the estuary and this influence deepens with increased wind speeds.

Morphological predictions made with tidal processes alone are complex with widely diverging morphologies emerging depending on the model and its setup (van Maanen et al., 2013a, Coco et al., 2013); factors such as initial conditions, sediment grain size or erosion thresholds can greatly impact the predicted morphological form. Including the effects of the wind-wave climate within this already complex modelling approach will be extremely difficult to achieve and will require careful application of the modelling results. The complexity is not only due to the variation in setup parameters (e.g. grid resolution, sediment parameterisation) but also due to the uncertainty of wave impacts on morphology and of future changes to climatic patterns such as those predicted to occur on the west coast of New Zealand. It is likely that future changes in wave generation and wind-driven circulation will need to be incorporated into predictions of estuarine morphology.

Acknowledgments

The funding for this PhD research was provided by the Commonwealth Doctoral Scholarship Award, the ASLO Global Outreach Initiative and the Terry Healy Memorial Award. Extensive and valuable field assistance was given by Dean Sandwell, Dirk Immenga, Dudley Bell, Phil Ross and Shawn Harrison from the University of Waikato. Data was also kindly provided by Waikato Regional Council. The Trustees of the Mai-Uenuku-ki-te-whenua Marae and the Trustees of Waingaro Pā gave helpful assistance, advice and guidance during the development of the fieldwork programme.

6 References

Augustinus, P.G.E.F. 1980. Actual development of the chenier coast of Suriname (South America). Sedimentary Geology, 26, pp. 91-113.

Bearman, J. A., Friedrichs, C. T., Jaffe, B. E. & Foxgrover, A. C. 2010. Spatial Trends in Tidal Flat Shape and Associated Environmental Parameters in South San Francisco Bay. Journal of Coastal Research, 26, 342-349.

Bentley, S.J., Swales, A., Pyenson, B. and Dawe, J. 2014. Sedimentation, bioturbation, and sedimentary fabric evolution on a modern mesotidal mudflat: A multi-tracer study of processes, rates and scales. Estuarine, Coastal and Shelf Science, 141, 58-68.

Bowers, D.G. and Al-Barakati, A. 1997. Tidal Rectification on Drying Estuarine Sandbanks. Estuaries, 20, No. 3, 559-568.

CERC. 1984. Shore Protection Manual, Volume 1. Waterways Experiment Station, Corps of Engineers, Coastal Engineering Research Center (CERC).

Coco, G., Zhou, Z., van Maanen, B., Olabarrieta, M., Tinoco, R. And Townend, I. 2013. Morphodynamics of tidal networks: Advances and challenges. Marine Geology, 346, pp. 1-16.

Dronkers, J. 1986. Tidal asymmetry and estuarine morphology. Netherlands Journal of Sea Research, 20, 117-131.

Fagherazzi, S., Carnielo, L., D'Alpaos, L. and Defina, A. 2006. Critical bifurcation of shallow microtidal landforms in tidal flats and salt marshes. PNAS, 103, no. 22, pp. 8337-8341.

Fagherazzi, S., Palermo, C., Rulli, M.C., Carniello, L. and Defina, A. 2007. Wind waves in shallow microtidal basins and the dynamic equilibrium of tidal flats. Journal of Geophysical Research, 112

Fagehrazzi, S., Hannion, M. and D'Odorico, P. 2008. Geomorphic structure of tidal hydrodynamics in salt marsh creeks. Water Resources Research, 44.

Fagherazzi, S. and Wiberg, P.L. 2009. Importance of wind conditions, fetch, and water levels on wave-generated shear stresses in shallow intertidal basins. Journal of Geophysical Research, 114

French, J.R., Burningham, H. and Benson, T. 2008. Tidal and Meteorological Forcing of Suspended Sediment Flux in a Muddy Mesotidal Estuary. Estuaries and Coasts, 31, 843-859.

Friedrichs, C.T. & Aubrey, D.G. 1988. Non-linear Tidal Distortion in Shallow Well-mixed Estuaries: a Synthesis. Estuarine, Coastal and Shelf Science 27, pp. 521 – 545.

Friedrichs, C. T. & Aubrey, D. G. 1996. Uniform bottom shear stress and equilibrium hyposometry of intertidal flats. In: Pattiaratchi, C. B. (ed.) Mixing in Estuaries and Coastal Seas. Washington, DC: AGU.

Friedrichs, C. T. 2010. Barotropic tides in channelized estuaries. In: Valle-Levinson, A. (ed.) Treatise on Contemporary Issues in Estuarine Physics. Cambridge University Press, Cambridge, pp. 27-61.

Friedrichs, C. T. 2011. Tidal flat morphodynamics: a synthesis. In: Hansom, J. D. & Flemming, B. W. (eds.) Treatise on Estuarine and Coastal Science, Volume 3: Estuarine and Coastal Geology and Geomorphology. Elsevier.

Green, M.O., Black, K.P. and Amos, C.L. 1997. Control of estuarine dynamics by interactions between currents and waves at several scales. Marine Geology 144, pp. 97-116.

Green, M.O. 2011. Very small waves and associated sediment resuspension on an estuarine intertidal flat. Estuarine, Coastal and Shelf Science, 93, 449-459.

Green, M.O. and Coco, G. 2013. Review of wave-driven sediment resuspension and transport in estuaries. Reviews of Geophysics, 52.

Heath, R.A. 1976. Broad classification of New Zealand inlets with emphasis on residence times. New Zealand Journal of Marine and Freshwater Research. 10, 3, pp. 429-444

Henderson, S.M. and Mullarney, J.C. 2013. Wave mixed, wind-generated near-surface shear observed over a tidal flat. Continental Shelf Research, 60S, pp. S22-S29.

Hunt, S., Bryan, K.R. and Mullarney, J.C. 2015. The influence of wind and waves on the existence of stable intertidal morphology in meso-tidal estuaries. Geomorphology 228, pp. 158-174.

Janssen-Stedler, B. 2000. The effect of different hydrodynamic conditions on the morphodynamics of a tidal mudflat in the Dutch Wadden sea. Contenental Shelf Research, 20, 1461-1478.

Jones, N.L. and Monismith, S.G. 2007. Measuring short-period wind waves in a tidally forced environment with a subsurface pressure gauge. Limnology and Oceanography: Methods 5, pp.317-327.

Kirby, R. 2000. Practical Implications of tidal flat shape. Continental Shelf Research, 20, 1061-1077.

Kirby, R. 2002. Distinguishing accretion from erosion-dominated muddy coasts. In: Healy, T., Wang, H. and Healy, J.-A. (eds.) Muddy Coasts of the World: Processes Deposits and Function. Amsterdam: Elsevier Science B.V.

Lanzoni, S. And Seminara, G. 2002. Long-term evolution and morphodynamic equilibrium of tidal channels. Journal of Geophysical Research, 107, No. C1, pp. 1-13.

Mariotti, G. and Fagherazzi, S. 2012a. Channels-tidal flat sediment exchange: The channel spillover mechanism. Journal of Geophysical research, 117, C03032.

Mariotti, G. and Fagherazzi, S. 2012b. Modeling the effect of tides and waves on benthic biofilms. Journal of Geophysical research, 117.

Mariotti, G. And Fagherazzi, S. 2013a. A two-point model for the coupled evolution of channels and tidal flats. Journal of Geophysical research: Earth Surface, 118, pp. 1387-1399.

Mariotti, G. And Fagherazzi, S. 2013b. Wind waves on a mudflat: The influence of fetch and depth on bed shear stresses. Continental Shelf Research, 60S, pp.S99-S110

Mehta, A. J. 2002. Mudshore dynamics and controls. In: Healy, T., Wang, H. and Healy, J.-A. (eds.) Muddy Coasts of the World: Processes Deposits and Function. Amsterdam: Elsevier Science B.V.

McGlathery, K. J., Ridenbach, M. A., D'Odorico, P.,Fagherazzi, S., Pace, M. L. and Porter, J. H. Nonlinear Dynamics and Alternative Stable States in Shallow Coastal Systems. Oceanography, 26, No. 3.

Narváez, D.A. and Valle-Levinson, A. 2008. Transverse structure of wind-driven flow at the entrance to an estuary: Nansemond River. Journal of Geophysical Research, 113, C09004,1-9.

Pethick, J. S. 1994. Estuaries and wetlands: function and form. In: Falconer, R. A. and Goodwin, P. (eds.) Wetland Management. London: Thomas Telford Services Ltd.

Ranasinghe, R., McLoughlin, R., Short, A. And Symonds, G. 2004. The Southern Oscillation Index, wave climate, and beach rotation. Marine Geology, 204, pp. 273-287.

Roberts, W., Le Hir, P. & Whitehouse, R. J. S. 2000. Investigation using simple mathematical models of the effect of tidal currents and waves on the profile shape of intertidal mudflats. Continental Shelf Research, 20, 1079-1097.

Robins, P.E. and Davies, A.G. 2010. Morphological controls in sandy estuaries: the influence of tidal flats and bathymetry on sandy transport. Ocean Dynamics, 60, pp. 503-517.

Sanay, R. and Valle-Levinson, A. 2005. Wind-Induced Circulation in Semienclosed Homogenous, Rotating Basins. Journal of Physical Oceanography, 35, 2520-2531.

Sherwood, A.M. and Nelson, C.S. 1979. Surficial sediments of Raglan Harbour. New Zealand Journal of Marine and Freshwater Research, 13, 4, pp. 473-496.

Smith, M.J., Stevens, C.L., Gorman, R.M., McGregor, J.A. and Neilson, C.G. 2001. Wind-wave development across a large shallow intertidal estuary: a case study of Manukau Harbour, New Zealand. New Zealand Journal of Marne and Freshwater Research, 35, pp. 985-1000.

Souslby, R. 1997. Dynamics of Marine Sands: A Manual for Practical Applications. Published by Thomas Telford Publishing, London.

Swales, A., Ovenden, R., McGlone, M.S., Hermanspahn, N., Budd, R., Okey, M.J. and Hawken, J. 2005. Whaingaroa (Raglan) Harbour: sedimentation rates and the effects of historical catchment landcover changes. NIWA technical report for Environment Waikato. Technical report 2005/36.

Talke, S.A. and Stacey, M.T. 2008. Suspended sediment fluxes at an intertidal flat: The shifting influence of wave, wind, tidal and freshwater forcing. Continental Shelf Research, 28, pp. 710-725.

van Maanen, B., Coco, G. & Bryan, K.R. 2013a. Modelling the effects of tidal range and initial bathymetry on the morphological evolution of tidal embayments. Geomorphology, 191, pp. 23-34.

van Maanen, B., Coco, G., Bryan, K.R. & Friedrichs, C. T. 2013b. Modelling the morphodynamic response of tidal embayments to sea-level rise. Ocean dynamics, Volume 63, Issue 11-12, pp. 1249-1262.

van Maanen, B., Coco, G., Bryan, K.R. (2015). On the ecogeomorphological feedbacks that control tidal channel network evolution in a sandy mangrove setting. Proc. R. Soc. A 20150115. http://dx.doi.org/10.1098/rspa.2015.0115.

Waeles, B. T., Le Hir, P. & Silva Jacinto, R. 2004. Modélisation morphodynamique cross-shore d'un estran vaseux. Comptes Rendus Geoscience, 336, 1025-1033.

Wang, Z.B., Jeuken, M.C.J.L, Gerritsen, H., de Vriend, H.J. and Kornman, B.A. 2002. Morphology and asymmetry of the vertical tide in the Westerschelde estuary. Continental Shelf Research, pp.2599-2609.

Wells, J.T. and Coleman, J.M. 1981. Physical processes and fine-grained sedment dynamics, coast of Surinam, South America. Journal of sedimentary Petrology, 51, No. 4, pp. 1053-1068.

Whitehouse, R., Soulsby,R., Roberts, W. And Mitchener, H. 2000. Dynamics of Estuarine Muds: A Manual for Practical Applications. Published by Thomas Telford Publishing, London.

Wong, K-C. 1994. On the nature of transverse variability in a coastal plain estuary. Journal of Geophysical Research, 99, C7, 14, 209-14.

Woodroffe, C.D. 2002. Coasts. Form, process and evolution. Cambridge University Press.

Zhou, Z., Coco, G., van der Wegen, M., Ghong, Z., Zhang, C. and Townend, I. 2015. Modeling sorting dynamics of cohesive and non-cohesive sediments on intertidal flats under the effect of tides and wind waves. Continental Shelf Research, pp. 76-91.

Tables:

Table 1: Summary of instrumentation, deployment dates and parameters measured. See Figure 1 for locations of instruments.

Instrument	Map ID (Figure 1)	Deployment date	Retrieval date	Parameters	Sampling interval (s)	Sampling rate (Hz)	Sampling duration (s)	Averaging duration (s)
Weather Station (Taharoa)	●	10th August 1978	1st January 2013	Wind				
Weather Station (Raglan)	❋	30th April 2012	29th September 2013	Wind				
Sontek ADV	◊	24h October 2012	20th November 2012	Currents and water levels	600	1	120	120
Sontek ADV	◊	24h October 2012	20th November 2012	Waves	1800	4	256	NA
Sontek ADP	x	24th October 2012	20th November 2012	Currents and water levels	300	1	120	120
FSI current meter	+ (T1 profile)	16th October 2012	7th November 2012	Currents and water levels	600	5	60	60
Dobie	○ (T1	16th	7th	Waves	600	10	205	NA

wave gauge	profile)	October 2012	November 2012	and water levels				
OBS	∆ (T1 profile)	16th October 2012	7th November 2012	Suspended sediment	5	1	1	60
FSI current meter	+ (T2 profile)	8th November 2012	26th November 2012	Currents and water levels	600	5	60	60
Dobie wave gauge	○ (T2 profile)	8th November 2012	26th November 2012	Waves and water levels	600	10	205	NA
OBS	∆ (T2 profile)	8th November 2012	26th November 2012	Suspended sediment	5	1	1	60

Table 2: Influences of different hydrodynamic forcing due to frequency, type and magnitude of affect.

Frequency	*Semi-diurnal*	*Diurnal*	*Diurnal*	*Seasonal*
Physical process	*Tides*	*Sea breeze (circulation)*	*Sea breeze (waves)*	*Storms*
SSC	*Small*	*Small*	*Large*	*Very large*
Speed of change (based on SSC)	*Gradual*	*Gradual*	*Rapid*	*Very rapid*
Magnitude of change (relative to frequency, based on SSC)	*Small*	*Small*	*Moderate*	*Large*
Morphological impact	*Accretion*	*Accretion or erosion*	*Erosion*	*Erosion*

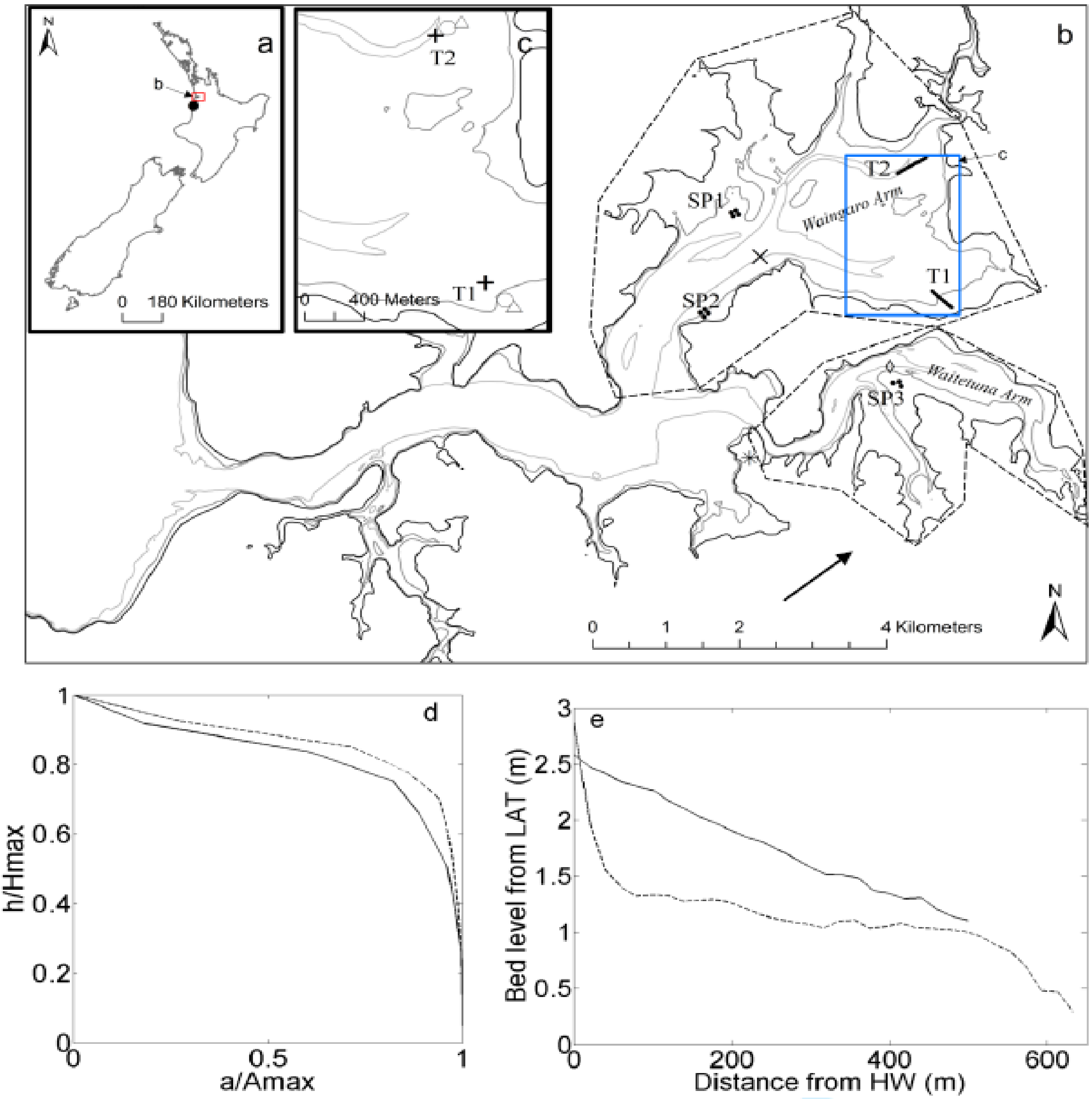

Figure 1: Location map showing location of Raglan (red square) and the Taharoa weather station (●) (a) and the field measurement locations (b). Inset (c) shows the area indicated by the blue box. The black, grey and light grey lines show the Highest Astronomical Tide, Mean Sea Level and Lowest Astronomical Tide depth contours. Dots show locations of sediment plate measurements SP1, SP2 and SP3. T1 and T2 show locations of instrument transects consisting of Optical Backscatter (Δ), current meter (+) and Dobie wave gauge (○). An Acoustic Doppler Velocimeter (◊) was deployed in the southern arm and an Acoustic Doppler Profiler (x) in the northern arm. A weather station was deployed in the main part of the estuary near the mouth of the southern arm (✳) and the arrow above the scalebar shows the strongest prevailing wind direction (from the SW). The dashed polygons define the approximate limits of each arm and the areas considered in the hypsometry calculations. (d) Hypsometric curves comparing area to height distribution for the northern (dashed thick line) and the southern (solid thick line) arms. (e) Depth profiles at the T1 (solid line) and T2 (dashed line) transects.

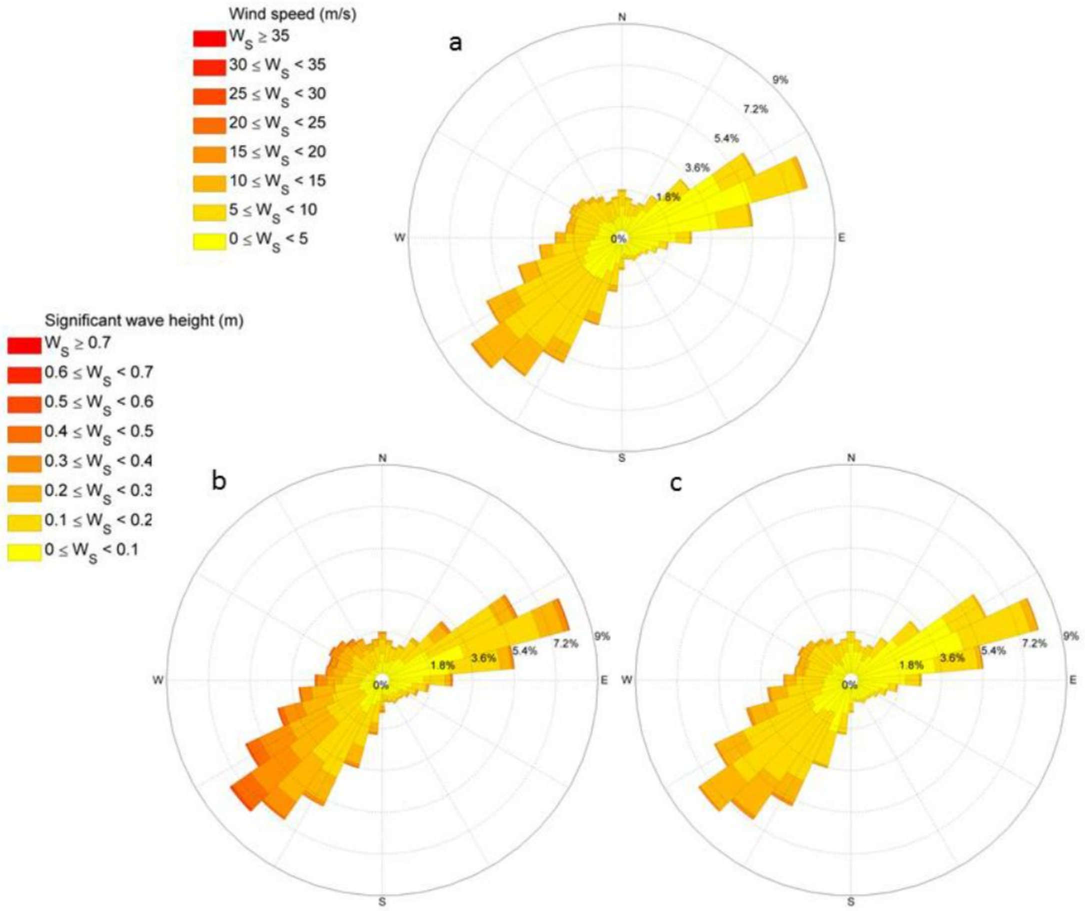

Figure 2: Wind rose showing the wind speed (denoted by colour), the wind direction (direction from, denoted by the orientation of the bars) and the frequency of occurrence (denoted by the length of each bar) (panel a), wind data are from Taharoa (see Figure 1a for location) collected between (10th August 1978 and 1st January 2013). Using fetch distances at high water from aerial photography, the wind records are converted into the distribution of predicted wave conditions for the Waingaro (panel b) and the Waitetuna (panel c) arms. Significant wave height, wind direction and the frequency of occurrence are denoted by the color, orientation and length of each bar, respectively.

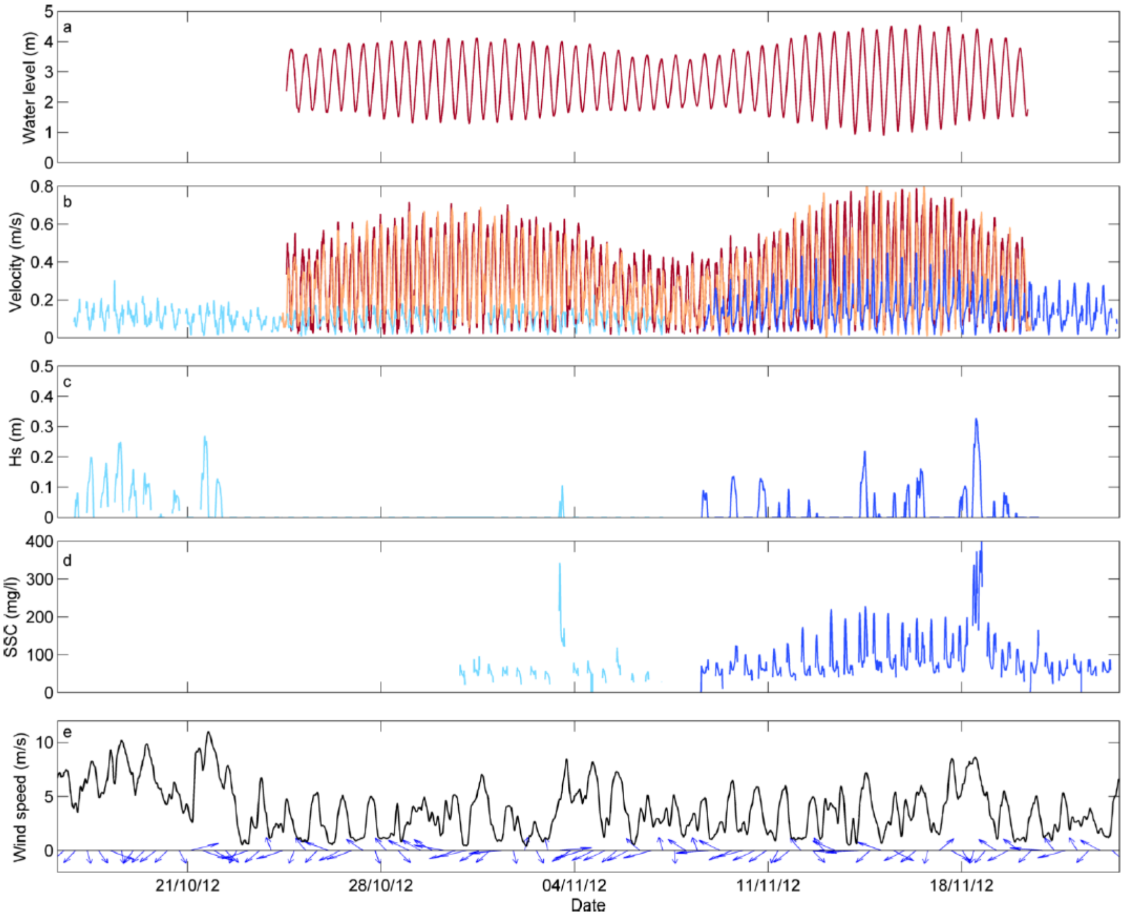

Figure 3: Timeseries collected during the field deployment. Locations of instruments are shown in Figure 1. Panel a shows water levels from the Acoustic Doppler Profiler (northern arm). Panel b shows depth averaged velocities from the northern arm (Acoustic Doppler Profiler in dark red and T1 and T2 in light and dark blue, respectively), and the Southern arm (Acoustic Doppler Velocimeter orange line). Panel c shows significant wave height at T1 (light blue) and T2 (dark blue). Panel d shows suspended sediment concentration measured using the lower sensor at T1 (light blue) and T2 (dark blue). Panel e shows the wind conditions measured at the Raglan weather station with speed (black line) and direction from (arrows).

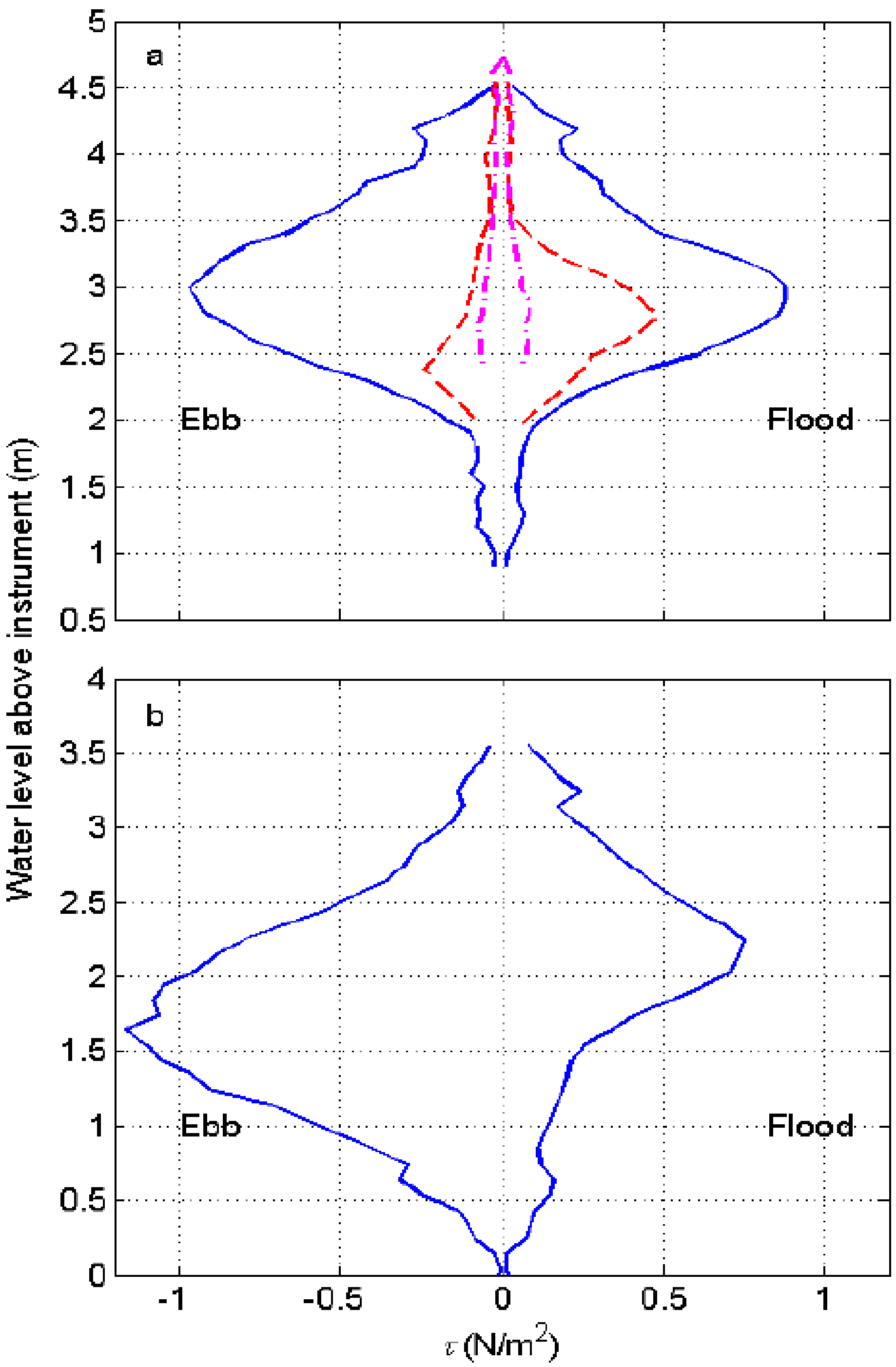

Figure 4: Tidal stage figures showing τ (bin averaged over entire deployment, with 0.1 m vertical resolution) plotted for each water level for the northern arm (a): Acoustic Doppler Profiler (solid line), T1 (dash-dotted line) and T2 deployments (dashed line); and the southern arm Acoustic Doppler Velocimeter (b).

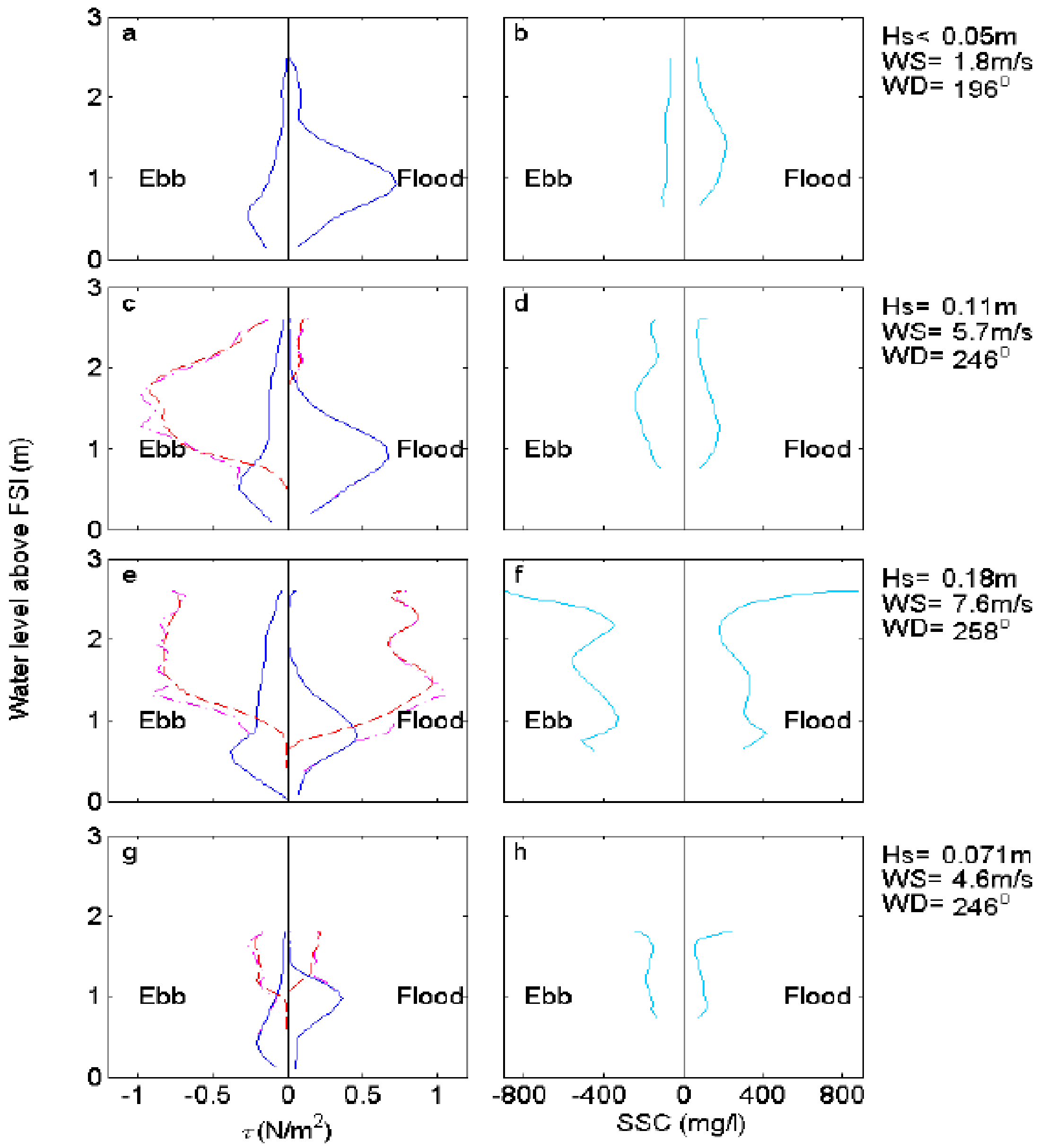

Figure 5: Tidal stage figures for (fetch-aligned) T2 deployment showing τ (solid line), τw (dashed line), τmax (dash-dotted line) and suspended sediment concentrations (SSC). Cases are shown for a tidal cycle with no waves (a and b), a tidal cycle during a spring tide and a moderate wind speed (c and d), a spring tide and a high wind speed (e and f) and a neap tide with a moderate wind speed (g and h). Mean significant wave height (Hs), wind speed (WS) and direction (WD) are shown for each case.

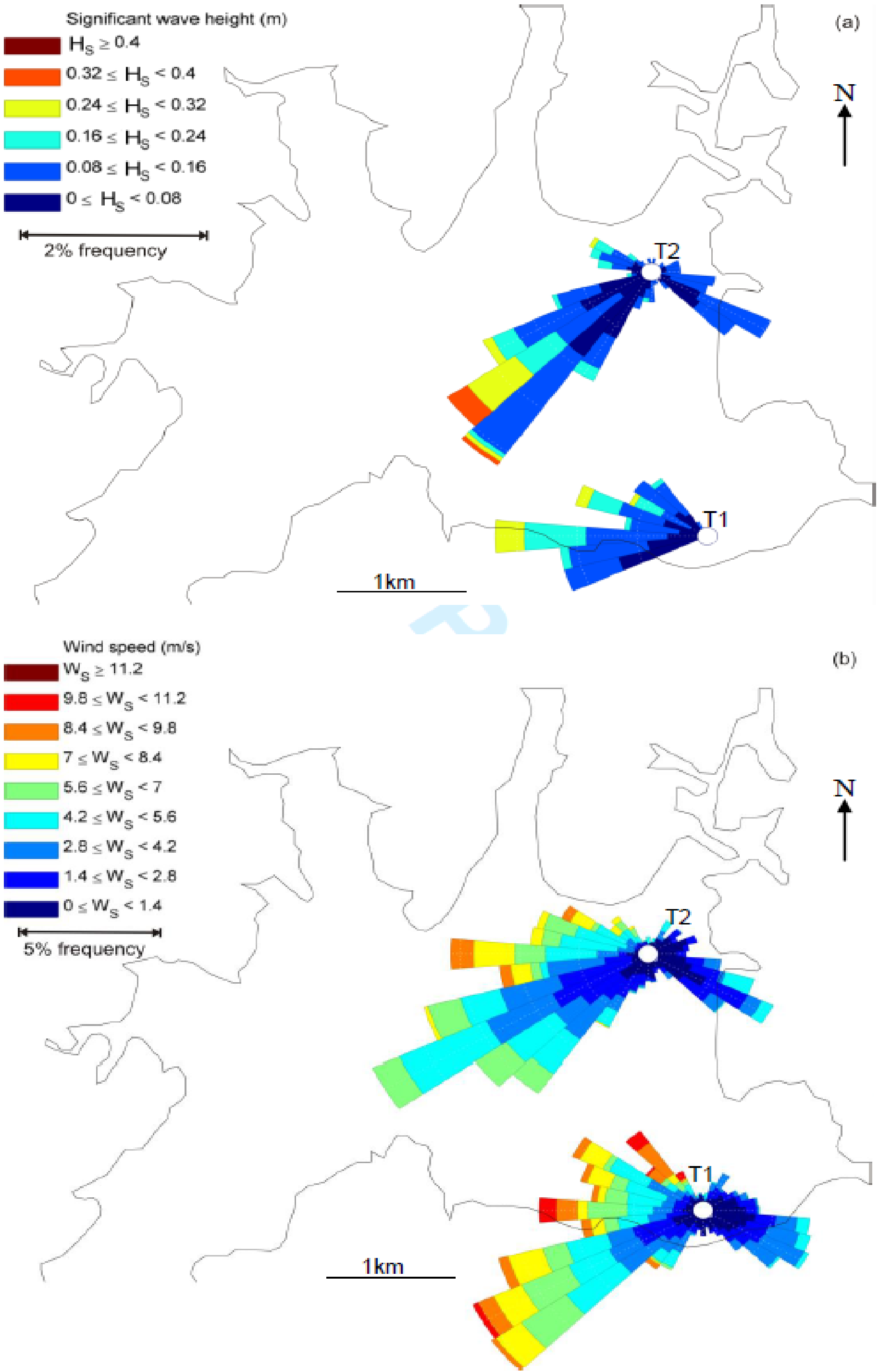

Figure 6: Panel a shows significant wave height (denoted by the colour) and frequency of occurrence (denoted by the length of each column relative to the scale bar) for each Dobie deployment. The direction of wind blowing during each wave event is taken from the Raglan weather station and is shown by the orientation of each column. Panel b shows the magnitude, frequency and direction of wind recorded at the Raglan weather station during each deployment.

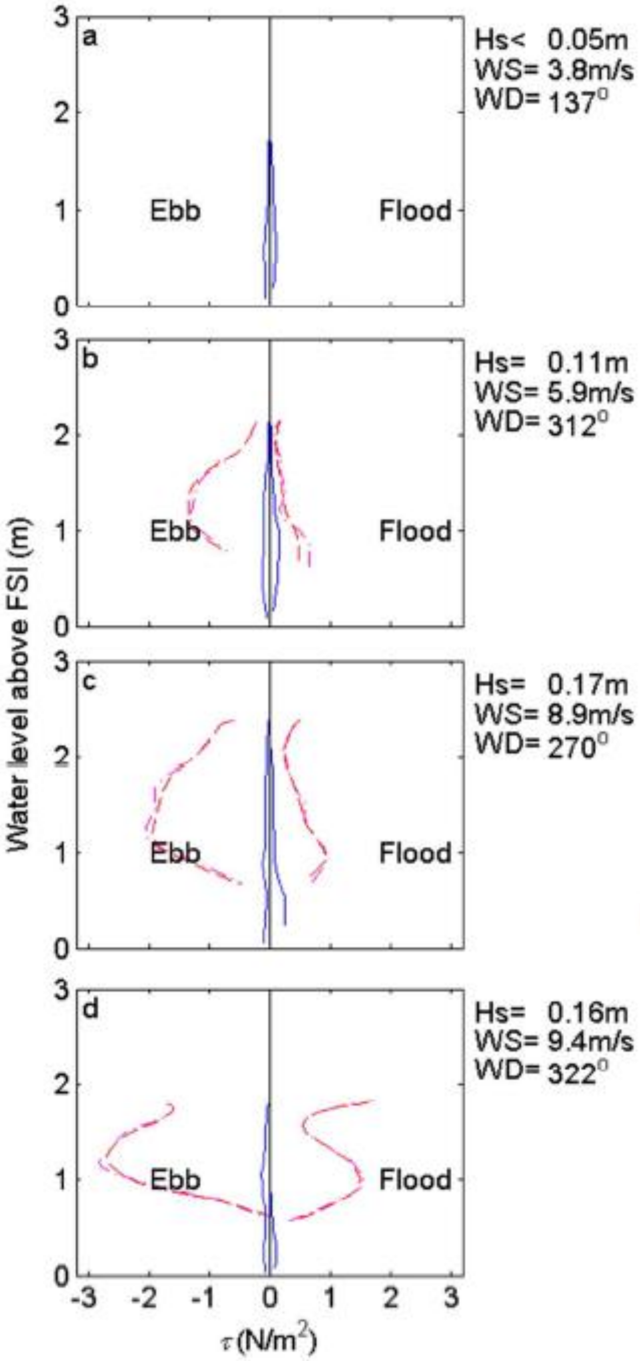

Figure 7: Tidal stage figures for the T1 deployment showing τ (solid line), τw (dashed line) and τmax (dash-dotted line). Cases shown are for a tidal cycle with no waves (a), a tidal cycle during a spring tide and a moderate wind speed (b), a spring tide and a high wind speed (c) and a neap tide with a moderate wind speed (d). Significant wave height, wind speed and direction are shown for each case. No suspended sediment concentrations are available for the T1 deployment due to instrument malfunction.

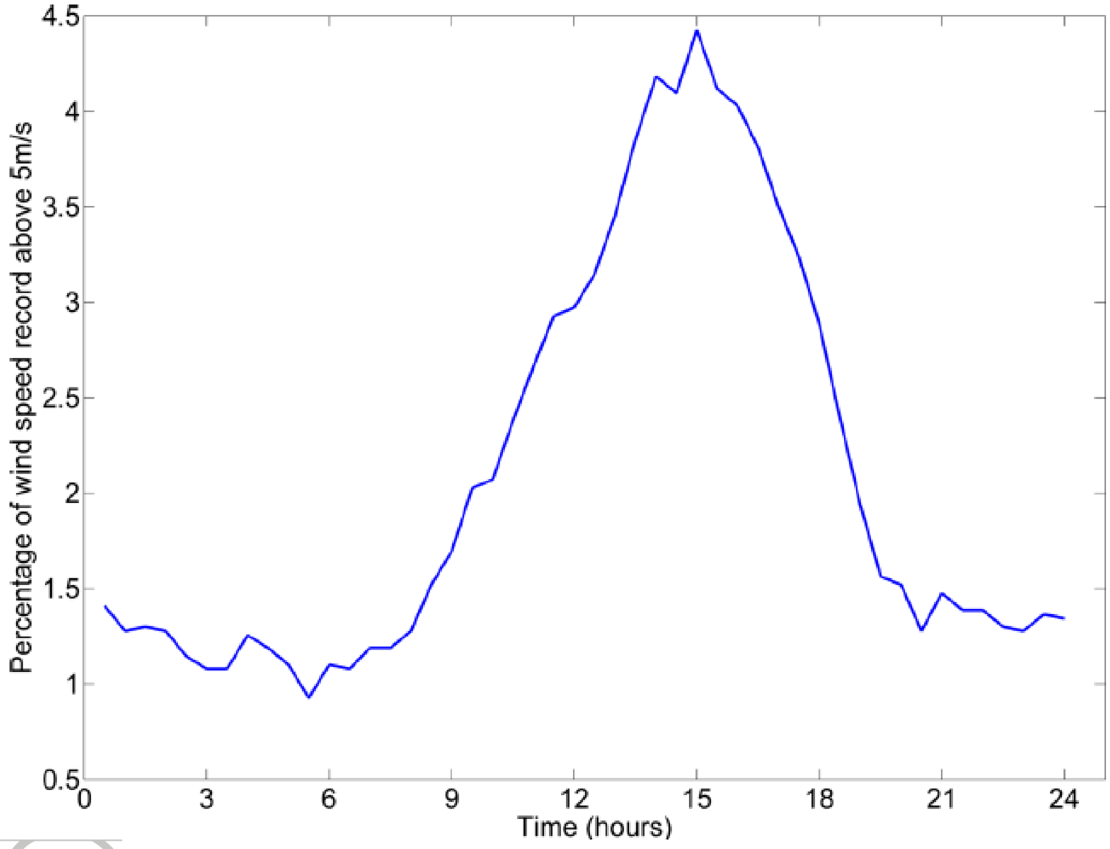

Figure 8: Occurrence of wind speeds above 5 m/s between 30th April 2012 and 29th September 2013 presented as percentage function of time of day.

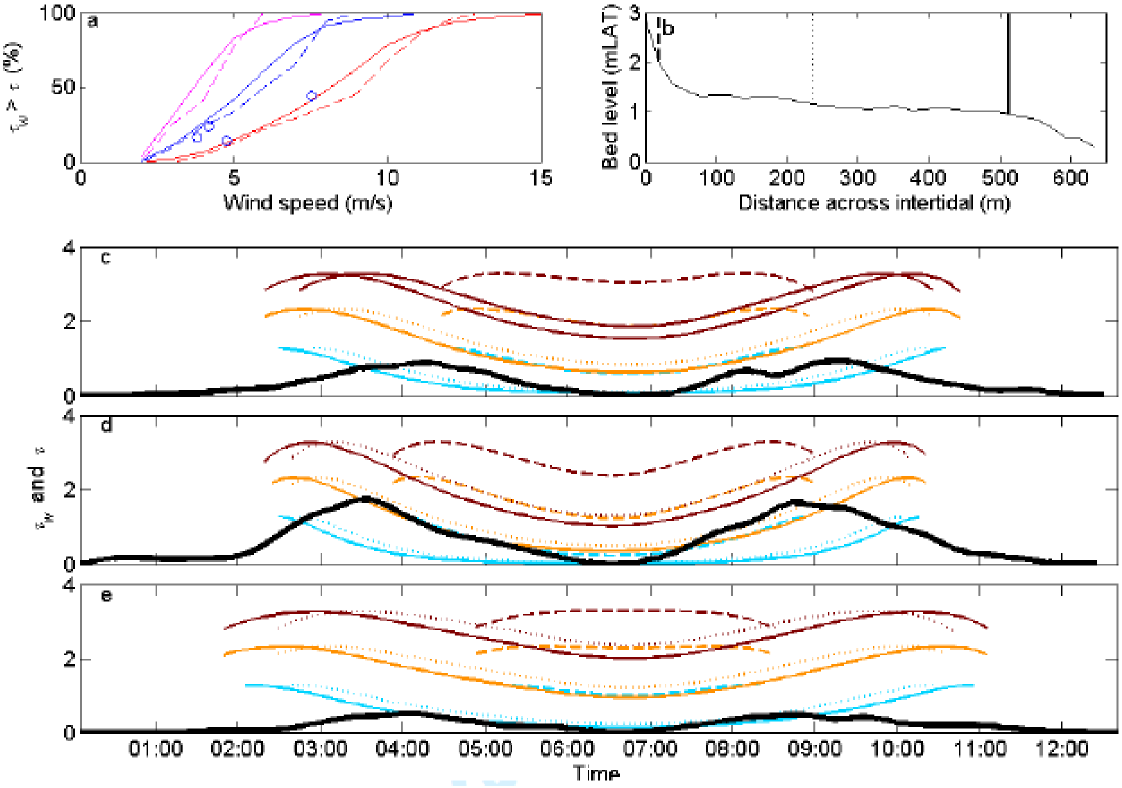

Figure 9: (a) Percentage of time when $\tau w > \tau$ over the entire intertidal area (solid lines) and at the location of the Dobie wave gauge (dashed lines) for neap (magenta), intermediate (blue)0 and spring (red) tides within an estuary with a maximum fetch of 5 km. Observations from the Dobie wave gauge are shown as circles. (b-d) Timeseries of τ in the channel (solid thick black line) against calculated τw (thin coloured lines) for intermediate (c), spring (d) and neap (e) tidal states. Wind speeds shown are 5 m/s (light blue), 10 m/s (orange) and 15 m/s (dark red) at the upper (dashed line), mid (dotted line) and lower (solid line) areas of the intertidal. The lower line is at the same location as the Dobie wave gauge, and the locations of the data points within the intertidal profile are shown in b.

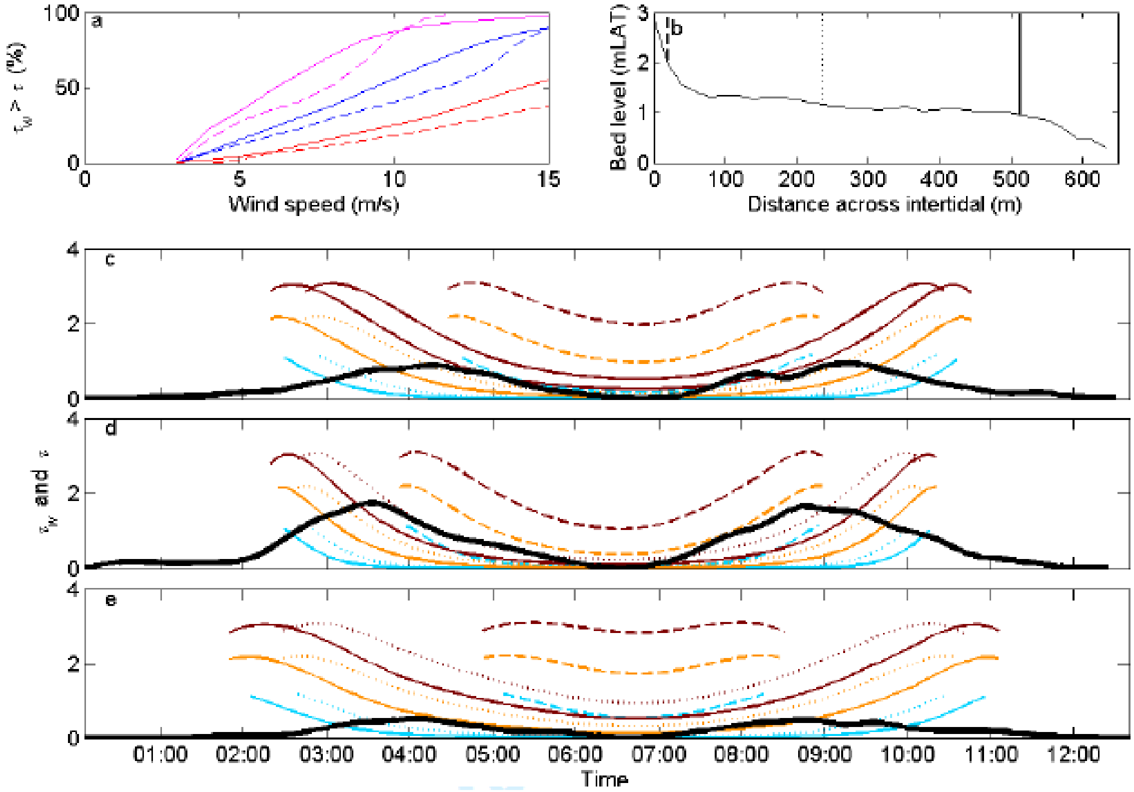

Figure 10: (a) Percentage of time when $\tau w > \tau$ over the entire intertidal area (solid lines) and at the location of the Dobie wave gauge (dashed lines) for neap (magenta), intermediate (blue) and spring (red) tides within an estuary with a maximum fetch of 2 km. (b-d) Timeseries of τ in the channel (solid thick black line) against calculated τw (thin coloured0 lines) for intermediate (c), spring (d) and neap (e) tidal states. Wind speeds shown are 5 m/s (light blue), 10 m/s (orange) and 15 m/s (dark red) at the upper (dashed line), mid (dotted line) and lower (solid line) areas of the intertidal. The locations of the data points within the intertidal profile are shown in b.

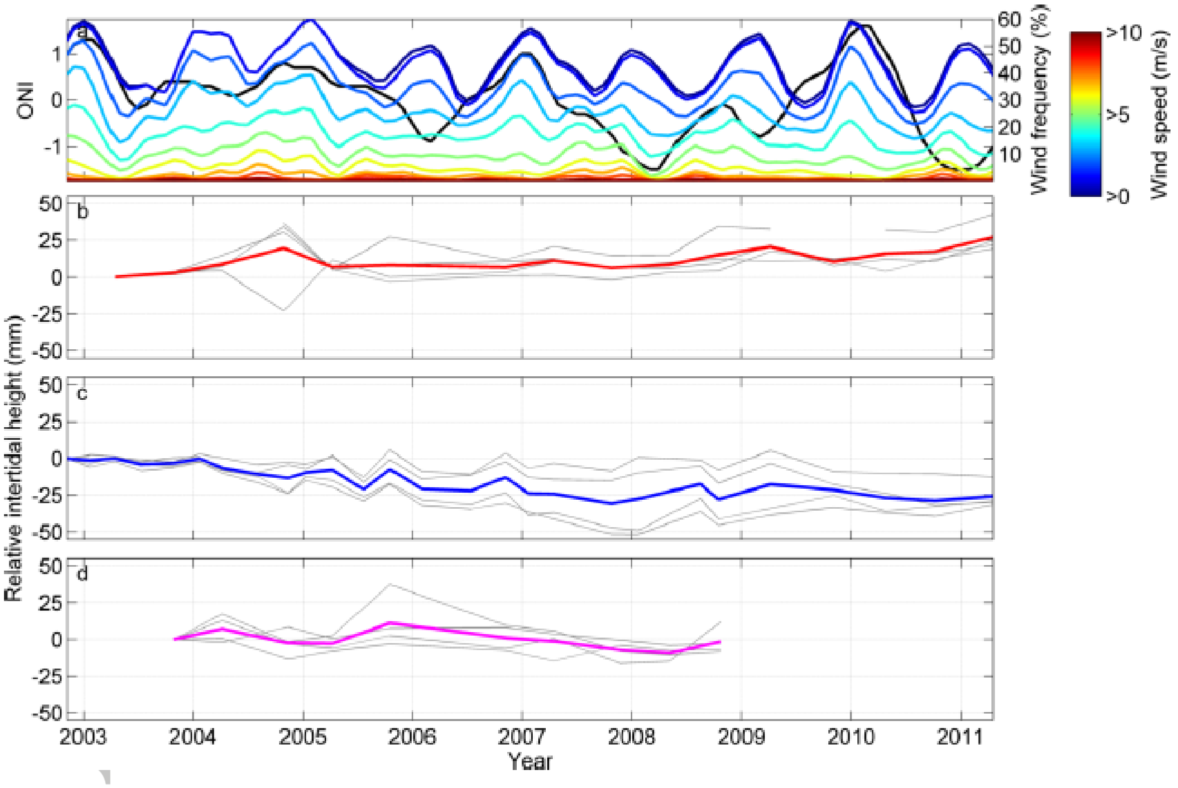

Figure 11: Three month running average of NOAA Oceanic Nino Index (ONI, black line), occurrence of south westerly winds (coloured by speed) as a percentage (panel a). Positive ONI denotes El Niño and negative donates La Niña and the index is considered significant by NOAA when >0.5 and <-0.5. Sediment plate data showing relative sediment depth (adjusted relative to first measurement) at each plate with coloured line showing mean of results for SP3, southern arm (panel b), SP1 (panel c) and SP2, northern arm (panel d). Wind data are from Taharoa weather station (see Figure 1a for location) modified according to the wind data collected in the Raglan Harbour.